Physica **98A** (1979) 41–86 © *North-Holland Publishing Co.*

THE INFLUENCE OF A MAGNETIC FIELD ON THE THERMAL DIFFUSION OF POLYATOMIC GAS–NOBLE GAS MIXTURES

G.W. 'T HOOFT, E. MAZUR, J.M. BIENFAIT, L.J.F. HERMANS, H.F.P. KNAAP AND J.J.M. BEENAKKER

Huygens Laboratorium der Rijksuniversiteit, Leiden, The Netherlands

Received 21 March 1979

Experiments on the influence of a magnetic field on the thermal diffusion (D_T) have been performed. Both the transverse coefficient, D_T^{tr}, as well as the difference between the longitudinal coefficients, $D_T^{\perp} - D_T^{\parallel}$, were measured for binary mixtures of N_2, nD_2, HD and nH_2 with the noble gases Ar, Ne and He and for the system pH_2–Ar. For most of these systems, the results can be adequately described with the dominant angular momentum polarization of the form $W\overline{JJ}$. For some mixtures, however, a significant contribution from a second polarization (viz. WJ) was found to be present. The results are expressed in terms of effective molecular cross sections. Using these results and those earlier obtained for the magnetic field effect on the thermal conductivity, an estimate is made about the magnitude of the Senftleben–Beenakker effect on the diffusion.

1. Introduction

The influence of external fields on the transport properties of polyatomic gases (Senftleben–Beenakker effect) provides information on collision processes of rotating molecules. For a survey see e.g., refs. 1–5. The Senftleben–Beenakker effect can be understood as follows: In a nonequilibrium situation, gradients in macroscopic properties (e.g., ∇T) produce anisotropies not only in velocity space, but – through collisions – also in angular momentum, J, space. For the production of such angular momentum dependent polarizations, the nonspherical part of the intermolecular interaction is responsible. In an external field, the angular momentum polarizations are partially destroyed by the precession of J around the field. This, in turn, will influence the transport properties.

The Senftleben–Beenakker effect has been extensively studied over the last decades. It was found that a gradient in the stream velocity generates

predominantly a tensor polarization of the type JJ, whereas a temperature gradient produces predominantly a vector polarization of the type $W \cdot JJ$. Here, W is the reduced peculiar velocity. However, the simple description on the basis of the $W \cdot JJ$ polarization only was found to be inadequate for many gases. In these cases two polarizations ($W \cdot JJ$ and $W \wedge J$) are needed to obtain agreement between theory and experiment. For a survey of recent work see refs. 6 and 7.

Observation of the field effects on diffusion and thermal diffusion proved to be difficult in the past. For thermal diffusion[8,9]), this might not seem surprising since thermal diffusion is a small effect itself, being a cross effect between heat transport and particle flux. For the relative change of the diffusion[10,11]), however, the upper limit 0.02% reported in the literature seems surprisingly low, since one would intuitively expect an effect of the same order of magnitude as for viscosity and thermal conductivity (i.e., 0.1–1%). For the case of thermal diffusion in an electric field, experimental results have been reported[12]).

Experimental data for the field effect on thermal diffusion are quite useful. First, they give new information on the coupling between the angular momentum polarization and the particle flux. Secondly, such data may clarify the deviations observed in the thermal conductivity experiments discussed above, since in both experiments the polarizations are the same, being produced by a temperature gradient in each case. Finally such data make it possible to predict the magnitude of the field effect on diffusion by making use of a relation between the field effects on diffusion, thermal diffusion and thermal conductivity. To verify this relation the experimental study of the diffusiomagnetic effect is undertaken and preliminary data are now at hand[13]).

In this paper, data will be reported on the magnetic field influence on the thermal diffusion for the binary mixtures of N_2, HD, nH_2 and nD_2 with Ar, Ne and He, and for the system pH_2–Ar at 300 K and at various concentrations.

2. Principle of the experiment

In a binary gas mixture, a particle flux can be generated by a concentration gradient (diffusion) as well as by a temperature gradient (thermal diffusion, for liquids sometimes called Soret effect). When no external forces or pressure gradients are present, the (pressure independent) flux of species A is in the field free case given by

$$j_A = -nD_{T_A} \nabla \ln T - nD \nabla x_A, \tag{1}$$

where n is the total number density, $x_A = n_A/n$ is the mole fraction, and D_{T_A}

and D are the thermal diffusion coefficient and the diffusion coefficient respectively. An analogous equation holds for component B of the mixture. If a constant temperature gradient is applied, the resulting concentration gradient in the steady state ($j_A = 0$) is therefore given by

$$\nabla x_A = -D^{-1} D_{T_A} \nabla \ln T, \tag{2}$$

where $D^{-1}D_{T_A}$ is often called the thermal diffusion ratio, k_T. To compensate for the main concentration dependence a thermal diffusion factor is defined as $\alpha = k_T/x_A x_B$. As seen from eq. (2), the concentration difference for small temperature differences is given in the steady state by

$$\Delta x_A = -k_T \Delta \ln T, \tag{3}$$

which is independent of the geometry. This concentration difference is quite small. As an example, for an equimolar N_2–Ar mixture at 300 K one finds $\Delta x = 6.0 \times 10^{-4}$ for $\Delta T = 10$ K.

Since $\nabla x_A = -\nabla x_B$ it follows from eq. (2) that

$$D_{T_A} = -D_{T_B}. \tag{4}$$

In the literature[14]) the convention is used that the species with greater mass has label A. Consequently, for $D_{T_A} > 0$, the particle flux of the heavy component is directed toward the cold side. This is the case for most gases at room temperature. In the studies of field effects on transport properties of mixtures, the convention has been used that the label A is given to the polyatomic molecule[15,16]). In this work we will adhere to this latter convention. As will be seen, there is no connection between the field effect on the thermal diffusion and the field free coefficient. Furthermore, no data on the field free coefficient will be used, so no misunderstanding will arise. For convenience, the subscript on D_T is dropped henceforth.

In a magnetic field, $\boldsymbol{B}$, the transport coefficients occurring in eq. (1) have to be replaced by tensors:

$$j_A = -n\boldsymbol{D}_T \cdot \nabla \ln T - n\boldsymbol{D} \cdot \nabla x_A. \tag{5}$$

Spatial symmetry considerations require that the thermal diffusion tensor takes the form

$$\boldsymbol{D}_T = \begin{pmatrix} D_T^{\perp} & -D_T^{tr} & 0 \\ D_T^{tr} & D_T^{\perp} & 0 \\ 0 & 0 & D_T^{\parallel} \end{pmatrix} \tag{6}$$

if the field is in the z-direction. The diagonal elements $D_T^{\parallel}$ and $D_T^{\perp}$ are even in the field, whereas D_T^{tr} is odd. For $B = 0$ one has $D_T^{\parallel} = D_T^{\perp} = D_T$ and $D_T^{tr} = 0$. For an evaluation of the experimental results it is desirable to measure at least

two independent (combinations of) elements of the transport tensor. Moreover, a high sensitivity will be required in view of the expected smallness of the concentration gradients to be detected. These two requirements are met by constructing a transverse type apparatus in which a field induced concentration gradient is detected perpendicular to the applied temperature gradient (see fig. 1). The resulting concentration difference δx depends on the geometry ($\delta x \propto l$) and can therefore be made arbitrarily large. Indeed, δx can be made even larger than Δx (see eq. (3)) which is independent of the geometry. It is clear from eq. (6) that the off-diagonal elements of the tensor will give rise to such a transverse effect, and that one measures D_T^{tr} when the field is perpendicular to ∇T (see fig. 1a). It is, however, also possible to measure $D_T^{\parallel} - D_T^{\perp}$ if the field is orientated properly, which can be understood as follows. Consider a magnetic field under an angle $\pi/4$ with the temperature gradient (see fig. 1b), which is decomposed in a parallel and a perpendicular gradient. If $D_T^{\parallel}$ is different from $D_T^{\perp}$ the two concentration gradients $\nabla x_{\parallel}$ and $\nabla x_{\perp}$ are not the same. So the "total" concentration gradient will not have the same direction as the temperature gradient and have a component, δx, perpendicular to the temperature gradient.

The steady state solution of eq. (5) ($j_A = 0$) for the orientation of magnetic field and temperature gradient of fig. 1a is

$$\nabla x_A = \left[\frac{D^{\perp} D_T^{tr}}{(D^{\perp})^2 + (D^{tr})^2} - \frac{D^{tr} D_T^{\perp}}{(D^{\perp})^2 + (D^{tr})^2}\right] \nabla \ln T, \tag{7}$$

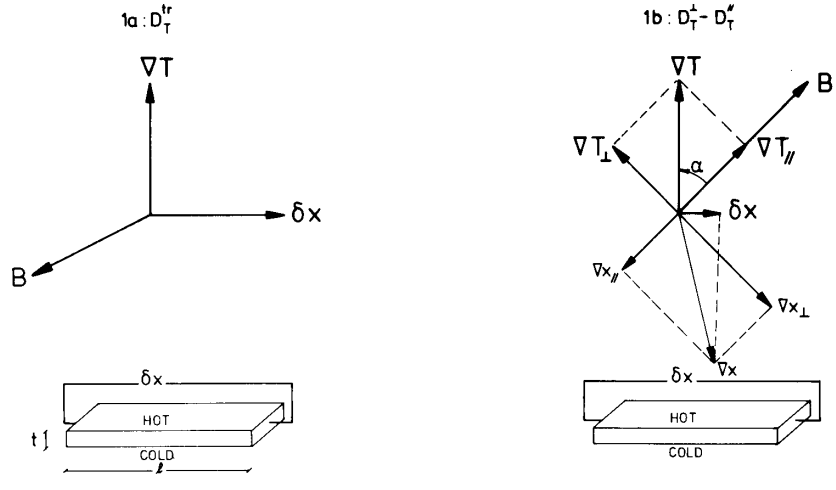

Fig. 1. a. The physical significance of the thermal diffusion coefficient D_T^{tr} in a magnetic field (note that in the absence of the field $D_T^{tr} = 0$). b. The physical significance of the difference between the thermal diffusion coefficients $D_T^{\parallel}$ and $D_T^{\perp}$ in a magnetic field (note that in the absence of the field $D_T^{\parallel} = D_T^{\perp} = D_T$).

NORTH-HOLLAND PHYSICA A VOL 98a NO 1 + 2 VEL 3

and for the orientation of fib. 1b, with α the angle between ∇T and $\boldsymbol{B}$:

$$\nabla x_A = -\sin\alpha\cos\alpha\left[\frac{D_T^{/\!/}}{D^{/\!/}} - \frac{D^{\perp}D_T^{\perp}}{(D^{\perp})^2+(D^{tr})^2} - \frac{D_T^{tr}D^{tr}}{(D^{\perp})^2+(D^{tr})^2}\right]\nabla \ln T. \tag{8}$$

It is seen from eq. (8) that the largest concentration gradient is obtained when $\alpha = \pi/4$. Since the magnetic field only slightly changes the transport coefficient, one has $D^{tr} \ll D$, $D^{\perp} \approx D^{/\!/} \approx D$. Furthermore, for most gas mixtures the field free thermal diffusion ratio k_T is of the order of 0.01 and D^{tr}/D_T^{tr} is of the order of unity (see ref. 17 and section 11). Therefore, the last terms of eqs. (7) and (8) can be neglected, so that one gets for the transverse concentration gradient in the case of fig. 1a

$$\delta x_A = \frac{l}{t}\frac{D_T^{tr}}{D}\Delta \ln T \tag{9}$$

and in the case of fig. 1b with $\alpha = \pi/4$:

$$\delta x_A = \frac{l}{t}\frac{D_T^{\perp} - D_T^{/\!/}}{2D}\Delta \ln T. \tag{10}$$

Here t and l are the distances over which the temperature gradient and transverse concentration gradient exist respectively.

3. Theory

The field influence on the thermal diffusion has been theoretically studied by several investigators: In kinetic theory, Kagan and Maksimov[18]), and also Eggermont, Vestner and Knaap[17]) used an inverse operator technique, whereas Köhler and Halbritter[19]) used the moment method. A treatment of the influence of the electric field on thermal diffusion was given by Borman et al.[20]). It is noted, that Monchick et al.[21]) have calculated the thermal diffusion factor with extra terms concerning the internal degrees of freedom which vanish when the interaction potential is spherical. In this section theoretical expressions relevant for the magnetic field effect on thermal diffusion will be given. For a detailed outline of the theory the reader is referred to Eggermont et al.[17]).

In experiments on the influence of a magnetic field on the thermal conductivity[7,15,22,23]) the only polarizations depending on $\boldsymbol{J}$ observed are $\boldsymbol{WJ}$ and $\overline{\boldsymbol{WJJ}}$, here the symbol $\overline{}$ denotes the symmetric traceless part of the tensor. Taking only these polarizations into account in the case of thermal diffusion is justified by the fact that in both type of experiments the polarizations are caused by a thermal gradient. Now the elements of the thermal diffusion

tensor change in the presence of a magnetic field according to

$$\frac{D_{\mathrm{T}}^{\mathrm{tr}}}{D} = \Psi_{11}^{\mathrm{T}} \frac{\xi_{11}}{1+\xi_{11}^2} - \Psi_{12}^{\mathrm{T}}\left(\frac{\xi_{12}}{1+\xi_{12}^2} + 2\frac{2\xi_{12}}{1+4\xi_{12}^2}\right),$$

$$\frac{\Delta D_{\mathrm{T}}^{\perp}}{D} = \frac{D_{\mathrm{T}}^{\perp}(B) - D_{\mathrm{T}}(0)}{D} = \Psi_{11}^{\mathrm{T}} \frac{\xi_{11}^2}{1+\xi_{11}^2} - \Psi_{12}^{\mathrm{T}}\left(\frac{\xi_{12}^2}{1+\xi_{12}^2} + 2\frac{4\xi_{12}^2}{1+4\xi_{12}^2}\right),$$

$$\frac{\Delta D_{\mathrm{T}}^{\parallel}}{D} = \frac{D_{\mathrm{T}}^{\parallel}(B) - D_{\mathrm{T}}(0)}{D} = 2\Psi_{11}^{\mathrm{T}} \frac{\xi_{11}^2}{1+\xi_{11}^2} - 2\Psi_{12}^{\mathrm{T}} \frac{\xi_{12}^2}{1+\xi_{12}^2}, \tag{11}$$

from which it follows that

$$\frac{D_{\mathrm{T}}^{\perp}(B) - D_{\mathrm{T}}^{\parallel}(B)}{2D} = -\frac{1}{2}\Psi_{11}^{\mathrm{T}} \frac{\xi_{11}^2}{1+\xi_{11}^2} + \Psi_{12}^{\mathrm{T}}\left(\frac{1}{2}\frac{\xi_{12}^2}{1+\xi_{12}^2} - \frac{4\xi_{12}^2}{1+4\xi_{12}^2}\right),$$

with the field parameter

$$\xi_{pq} = \frac{g\mu_{\mathrm{N}}kT}{\hbar}\{x_A v_{AA}\mathfrak{S}\left(\begin{smallmatrix} pq00 \\ pq00 \end{smallmatrix}\middle|\begin{smallmatrix} A \\ A \end{smallmatrix}\right)_{AA} + x_B v_{AB}\mathfrak{S}\left(\begin{smallmatrix} pq00 \\ pq00 \end{smallmatrix}\middle|\begin{smallmatrix} A \\ A \end{smallmatrix}\right)_{AB}\}^{-1}\frac{B}{p}, \quad pq = 11 \text{ or } 12^*. \tag{12}$$

Here g is the rotational g-factor of the polyatomic molecule, μ_{N} is the nuclear magneton and $v_{kl} = \sqrt{8kT(m_k+m_l)/\pi m_k m_l}$ is a thermal velocity. $\mathfrak{S}\left(\begin{smallmatrix} pq00 \\ pq00 \end{smallmatrix}\middle|\begin{smallmatrix} A \\ A \end{smallmatrix}\right)_{kl}$ are effective cross sections governing the decay of the polarization of rank p in $\boldsymbol{W}$ and q in $\boldsymbol{J}$ of molecule A, while concerning only collisions between species k and l. Analogous equations as (11) hold for $\boldsymbol{\lambda}$, the thermal conductivity tensor, $\boldsymbol{D}$, the diffusion tensor, $\mathscr{D}_{\mathrm{T}}$, the diffusion thermo (Dufour) tensor, with the same field parameters ξ_{11} and ξ_{12} but different magnitudes (Ψ_{pq}^{λ}, Ψ_{pq}^{D} and Ψ_{pq}^{τ} respectively) to be discussed in eqs. (13) through (17). As explained in section 2, $D_{\mathrm{T}}^{\mathrm{tr}}/D$ and $(D_{\mathrm{T}}^{\parallel} - D_{\mathrm{T}}^{\perp})/2D$ are investigated in this work. In fig. 2 the theoretical graphs of these two combinations of the elements of the thermal diffusion tensor are presented using eq. (11), while $\xi_{11} = \xi_{12}$ and $\Psi_{11}^{\mathrm{T}}/\Psi_{12}^{\mathrm{T}}$ is a parameter having the values -0.5, -0.2, 0, 0.2 and 0.5. For different ratios of Ψ_{11}^{T} and Ψ_{12}^{T} the actual shape of the curves does not change much. The ratio of $D_{\mathrm{T}}^{\mathrm{tr}}$ and $(D_{\mathrm{T}}^{\parallel} - D_{\mathrm{T}}^{\perp})/2$, however, does change drastically when $\Psi_{11}^{\mathrm{T}}/\Psi_{12}^{\mathrm{T}}$ is varied, since for decreasing values of $\Psi_{11}^{\mathrm{T}}/\Psi_{12}^{\mathrm{T}}$ the transverse effect is increased but the difference between the two longitudinal components decreases. The strengths of the polarizations, Ψ_{pq}, depend on effective molecular cross sections $\mathfrak{S}\left(\begin{smallmatrix} p\,q\,r\,s \\ p'q'r's' \end{smallmatrix}\middle|\begin{smallmatrix} k \\ l \end{smallmatrix}\right)_{kl}$. According to ref. 17 the Ψ_{pq}^{λ}, Ψ_{pq}^{T} and Ψ_{pq}^{D} are given by

$$\Psi_{pq}^{\lambda} = (1 - \tfrac{1}{2}\delta_{p1}\delta_{q2})\frac{k^2T}{m_A}\frac{\frac{1}{\lambda}\left[\sqrt{\frac{C_{\mathrm{rot}}^A}{k}}A - \sqrt{\frac{5}{2}}B\right]^2 x_A}{[x_A v_{AA}\mathfrak{S}\left(\begin{smallmatrix} pq00 \\ pq00 \end{smallmatrix}\middle|\begin{smallmatrix} A \\ A \end{smallmatrix}\right)_{AA} + x_B v_{AB}\mathfrak{S}\left(\begin{smallmatrix} pq00 \\ pq00 \end{smallmatrix}\middle|\begin{smallmatrix} A \\ A \end{smallmatrix}\right)_{AB}]}, \tag{13}$$

* The cross sections $\mathfrak{S}\left(\begin{smallmatrix} p\,q\,r\,s \\ p'q'r's' \end{smallmatrix}\middle|\begin{smallmatrix} A \\ A \end{smallmatrix}\right)_{AA}$ used in this work and refs. 17 and 24 correspond to the $\mathfrak{S}\left(\begin{smallmatrix} p\,q\,r\,s \\ p'q'r's' \end{smallmatrix}\right)_A$ of refs. 7, 15, 16 and 48.

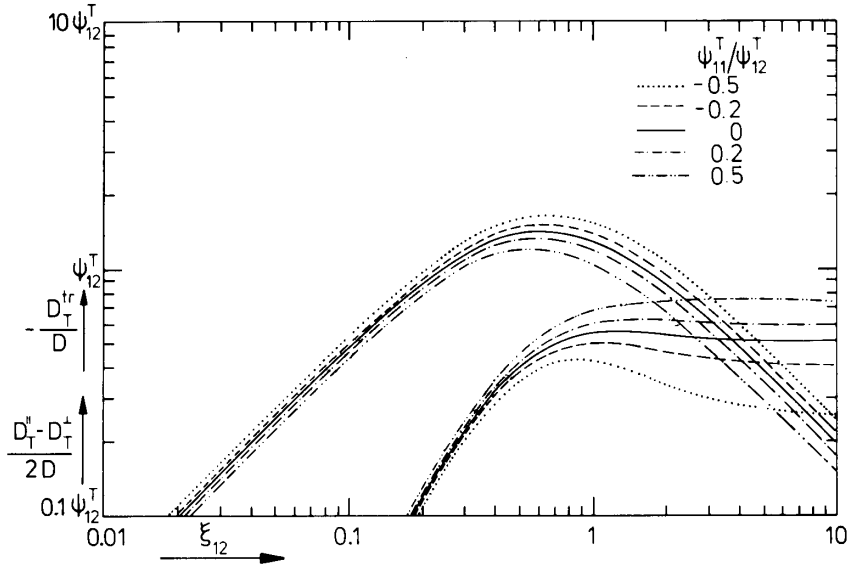

Fig. 2. The theoretical field dependence of D_T^{tr}/D and $(D_T^{\parallel}-D_T^{\perp})/2D$ according to eqs. (11), with $\xi_{11}=\xi_{12}$ and Ψ_{11}^T/Ψ_{12}^T having the values -0.5, -0.2, 0, 0.2 and 0.5.

$$\Psi_{pq}^T=(1-\tfrac{1}{2}\delta_{p1}\delta_{q2})\frac{x_Ax_Bv_{AB}\mathfrak{S}\left(\begin{smallmatrix}1000\\pq00\end{smallmatrix}\middle|\begin{smallmatrix}A\\A\end{smallmatrix}\right)_{AB}\left[\sqrt{\frac{C_{rot}^A}{k}}A-\sqrt{\frac{5}{2}}B\right]}{[x_Av_{AA}\mathfrak{S}\left(\begin{smallmatrix}pq00\\pq00\end{smallmatrix}\middle|\begin{smallmatrix}A\\A\end{smallmatrix}\right)_{AA}+x_Bv_{AB}\mathfrak{S}\left(\begin{smallmatrix}pq00\\pq00\end{smallmatrix}\middle|\begin{smallmatrix}A\\A\end{smallmatrix}\right)_{AB}]},\tag{14}$$

$$\Psi_{pq}^D=(1-\tfrac{1}{2}\delta_{p1}\delta_{q2})\frac{x_Bv_{AB}\mathfrak{S}^2\left(\begin{smallmatrix}1000\\pq00\end{smallmatrix}\middle|\begin{smallmatrix}A\\A\end{smallmatrix}\right)_{AB}}{\mathfrak{S}\left(\begin{smallmatrix}1000\\1000\end{smallmatrix}\middle|\begin{smallmatrix}A\\A\end{smallmatrix}\right)_{AB}[x_Av_{AA}\mathfrak{S}\left(\begin{smallmatrix}pq00\\pq00\end{smallmatrix}\middle|\begin{smallmatrix}A\\A\end{smallmatrix}\right)_{AA}+x_Bv_{AB}\mathfrak{S}\left(\begin{smallmatrix}pq00\\pq00\end{smallmatrix}\middle|\begin{smallmatrix}A\\A\end{smallmatrix}\right)_{AB}]}\tag{15}$$

with

$$A=\frac{x_Av_{AA}\mathfrak{S}\left(\begin{smallmatrix}1001\\pq00\end{smallmatrix}\middle|\begin{smallmatrix}A\\A\end{smallmatrix}\right)_{AA}+x_Bv_{AB}\mathfrak{S}\left(\begin{smallmatrix}1001\\pq00\end{smallmatrix}\middle|\begin{smallmatrix}A\\A\end{smallmatrix}\right)_{AB}}{x_Av_{AA}\mathfrak{S}\left(\begin{smallmatrix}1001\\1001\end{smallmatrix}\middle|\begin{smallmatrix}A\\A\end{smallmatrix}\right)_{AA}+x_Bv_{AB}\mathfrak{S}\left(\begin{smallmatrix}1001\\1001\end{smallmatrix}\middle|\begin{smallmatrix}A\\A\end{smallmatrix}\right)_{AB}},\tag{16}$$

$$\begin{aligned}B=&\Big\{[x_Av_{AA}\mathfrak{S}\left(\begin{smallmatrix}1010\\pq00\end{smallmatrix}\middle|\begin{smallmatrix}A\\A\end{smallmatrix}\right)_{AA}+x_Bv_{AB}\mathfrak{S}\left(\begin{smallmatrix}1010\\pq00\end{smallmatrix}\middle|\begin{smallmatrix}A\\A\end{smallmatrix}\right)_{AB}][x_Bv_{BB}\mathfrak{S}\left(\begin{smallmatrix}1010\\1010\end{smallmatrix}\middle|\begin{smallmatrix}B\\B\end{smallmatrix}\right)_{BB}\\&+x_Av_{AB}\mathfrak{S}\left(\begin{smallmatrix}1010\\1010\end{smallmatrix}\middle|\begin{smallmatrix}B\\B\end{smallmatrix}\right)_{AB}-x_B\sqrt{\frac{m_A}{m_B}}v_{AB}\mathfrak{S}\left(\begin{smallmatrix}1010\\1010\end{smallmatrix}\middle|\begin{smallmatrix}A\\B\end{smallmatrix}\right)_{AB}\Big]\\&+x_Bv_{AB}\mathfrak{S}\left(\begin{smallmatrix}1010\\pq00\end{smallmatrix}\middle|\begin{smallmatrix}B\\A\end{smallmatrix}\right)_{AB}\Big[-x_Av_{AB}\mathfrak{S}\left(\begin{smallmatrix}1010\\1010\end{smallmatrix}\middle|\begin{smallmatrix}A\\B\end{smallmatrix}\right)_{AB}+x_A\sqrt{\frac{m_A}{m_B}}v_{AA}\mathfrak{S}\left(\begin{smallmatrix}1010\\1010\end{smallmatrix}\middle|\begin{smallmatrix}A\\A\end{smallmatrix}\right)_{AA}\\&+x_B\sqrt{\frac{m_A}{m_B}}v_{AB}\mathfrak{S}\left(\begin{smallmatrix}1010\\1010\end{smallmatrix}\middle|\begin{smallmatrix}A\\A\end{smallmatrix}\right)_{AB}\Big]\Big\}\{[x_Av_{AA}\mathfrak{S}\left(\begin{smallmatrix}1010\\1010\end{smallmatrix}\middle|\begin{smallmatrix}A\\A\end{smallmatrix}\right)_{AA}\\&+x_Bv_{AB}\mathfrak{S}\left(\begin{smallmatrix}1010\\1010\end{smallmatrix}\middle|\begin{smallmatrix}A\\A\end{smallmatrix}\right)_{AB}][x_Bv_{BB}\mathfrak{S}\left(\begin{smallmatrix}1010\\1010\end{smallmatrix}\middle|\begin{smallmatrix}B\\B\end{smallmatrix}\right)_{BB}+x_Av_{AB}\mathfrak{S}\left(\begin{smallmatrix}1010\\1010\end{smallmatrix}\middle|\begin{smallmatrix}B\\B\end{smallmatrix}\right)_{AB}]\\&-x_Ax_Bv_{AB}^2\mathfrak{S}^2\left(\begin{smallmatrix}1010\\1010\end{smallmatrix}\middle|\begin{smallmatrix}A\\B\end{smallmatrix}\right)_{AB}\}^{-1}\end{aligned}\tag{17}$$

and $pq = 11, 12$.

Since diagonal cross sections of the form $\mathcal{S}\left(\begin{smallmatrix} pqrs \\ pqrs \end{smallmatrix} \middle| \begin{smallmatrix} l \\ l \end{smallmatrix}\right)_{lk}$ are positive, it is clear from eqs. (13), (14) and (15) that Ψ^{λ}_{pq} and Ψ^{D}_{pq} are also positive, while Ψ^{T}_{pq} can have either sign. So when the $\boldsymbol{WJJ}$-polarization is dominant, the parallel and perpendicular components of the thermal conductivity and diffusion tensor will decrease in the presence of a magnetic field, while those of the thermal diffusion tensor need not do so.

In eqs. (13) through (17) off-diagonal cross sections of the form $\mathcal{S}\left(\begin{smallmatrix} pqrs \\ p'q'r's' \end{smallmatrix} \middle| \begin{smallmatrix} l \\ k \end{smallmatrix}\right)$ have been neglected with respect to diagonal ones. The justification of this approximation is that the cross section $\mathcal{S}\left(\begin{smallmatrix} 1010 \\ 1001 \end{smallmatrix} \middle| \begin{smallmatrix} A \\ A \end{smallmatrix}\right)_{AA}$ is purely inelastic and, in the lowest order Distorted Wave Born Approximation, the contributions to $\mathcal{S}\left(\begin{smallmatrix} 1010 \\ 1001 \end{smallmatrix} \middle| \begin{smallmatrix} A \\ A \end{smallmatrix}\right)_{AB}$, $\mathcal{S}\left(\begin{smallmatrix} 1010 \\ 1001 \end{smallmatrix} \middle| \begin{smallmatrix} B \\ A \end{smallmatrix}\right)_{AB}$ and $\mathcal{S}\left(\begin{smallmatrix} 1000 \\ 1001 \end{smallmatrix} \middle| \begin{smallmatrix} A \\ A \end{smallmatrix}\right)_{AB}$ are second order in the non-sphericity. (With inelastic is meant: only those collisions contribute in which the total internal energy of the two colliding molecules changes.) So these cross sections are expected to be small with respect to diagonal cross sections (which have elastic contributions). The only off-diagonal cross sections which have elastic contributions are $\mathcal{S}\left(\begin{smallmatrix} 1000 \\ 1010 \end{smallmatrix} \middle| \begin{smallmatrix} A \\ A \end{smallmatrix}\right)_{AB}$ and $\mathcal{S}\left(\begin{smallmatrix} 1000 \\ 1010 \end{smallmatrix} \middle| \begin{smallmatrix} A \\ B \end{smallmatrix}\right)_{AB}$. It will now be shown that these cross sections are also small:

They are related by (see ref. 24 and table VIII)

$$\mathcal{S}\left(\begin{smallmatrix} 1000 \\ 1010 \end{smallmatrix} \middle| \begin{smallmatrix} A \\ A \end{smallmatrix}\right)_{AB} = -\left(\frac{m_B}{m_A}\right)^{3/2} \mathcal{S}\left(\begin{smallmatrix} 1000 \\ 1010 \end{smallmatrix} \middle| \begin{smallmatrix} A \\ B \end{smallmatrix}\right)_{AB}. \tag{18}$$

The elastic contributions zeroth order in the nonsphericity, can be related to the well-known Chapman and Cowling Ω-integrals[25,26]) by

$$\mathcal{S}^{(0)}\left(\begin{smallmatrix} 1000 \\ 1010 \end{smallmatrix} \middle| \begin{smallmatrix} A \\ B \end{smallmatrix}\right)_{AB} = \frac{4}{3}\sqrt{\frac{2}{5}} \frac{m_A^{3/2} m_B^{1/2}}{(m_A + m_B)^2} (3\Omega^{*(1,2)}_{AB} - \tfrac{5}{2}\Omega^{*(1,1)}_{AB}) \pi \sigma^2_{AB}. \tag{19}$$

Using the data for the potential parameters, and the collision integrals of ref. 26 the cross sections $\mathcal{S}\left(\begin{smallmatrix} 1000 \\ 1010 \end{smallmatrix} \middle| \begin{smallmatrix} A \\ B \end{smallmatrix}\right)_{AB}$ are calculated for mixtures of N_2, HD, H_2 and D_2 with He, Ne and Ar. The results are shown in table I. For comparison the diagonal cross section $\mathcal{S}\left(\begin{smallmatrix} 1010 \\ 1010 \end{smallmatrix} \middle| \begin{smallmatrix} A \\ A \end{smallmatrix}\right)_{AA}$ and the off-diagonal cross section

TABLE I
Comparison of off-diagonal cross sections

	$\mathcal{S}\left(\begin{smallmatrix} 1010 \\ 1001 \end{smallmatrix} \middle| \begin{smallmatrix} A \\ A \end{smallmatrix}\right)_{AA}$ (10^{-20} m^2)	$-\mathcal{S}^{(0)}\left(\begin{smallmatrix} 1000 \\ 1010 \end{smallmatrix} \middle| \begin{smallmatrix} A \\ B \end{smallmatrix}\right)_{AB}$ (10^{-20} m^2)			$\mathcal{S}\left(\begin{smallmatrix} 1010 \\ 1010 \end{smallmatrix} \middle| \begin{smallmatrix} A \\ A \end{smallmatrix}\right)_{AA}$ (10^{-20} m^2)
		He	Ne	Ar	
N_2	4.0 [7])	1.9	2.0	1.5	27 [7])
HD	0.58 [7])	1.0	0.24	0.12	13 [7])
H_2	0.045 [7])	0.75	0.14	0.067	13 [7])
D_2	0.076 [7])	1.2	0.33	0.17	13 [7])

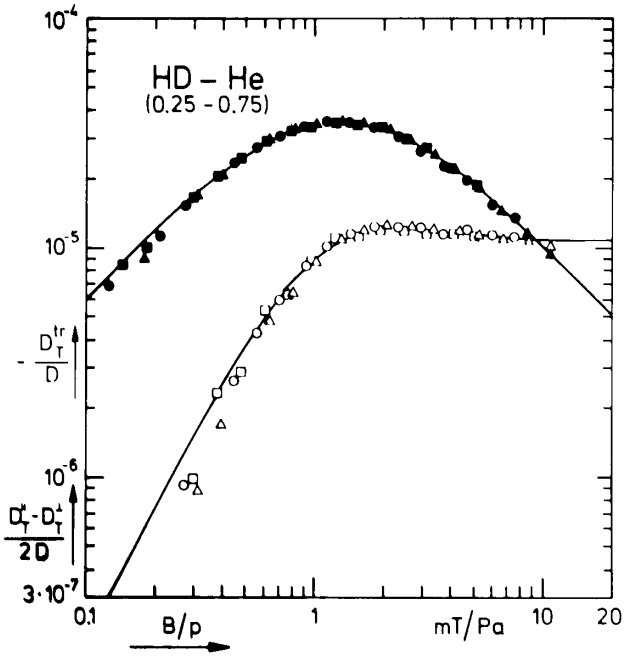

Fig. 14. $-D_T^{tr}/D$ and $(D_T^{\parallel} - D_T^{\perp})/2D$ versus B/p for HD–He ($x_{\text{noble gas}} = 0.75$); ▲△ 186.7 Pa; ●○ 267.3 Pa; ■□ 399.6 Pa; —— theoretical curves of eqs. (11) fitted to the experimental points.

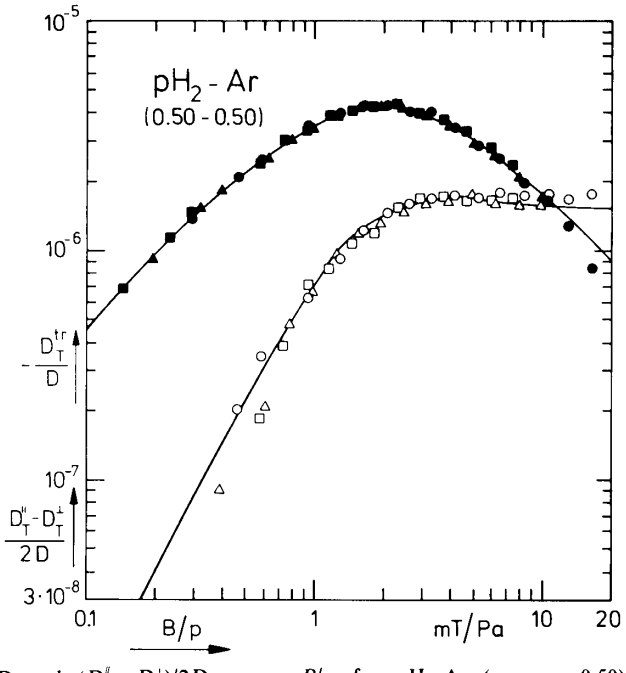

Fig. 15. $-D_T^{tr}/D$ and $(D_T^{\parallel} - D_T^{\perp})/2D$ versus B/p for pH_2–Ar ($x_{\text{noble gas}} = 0.50$); ●○ 133.9 Pa; ▲△ 199.6 Pa; ■□ 267.6 Pa; —— theoretical curves of eqs. (11) fitted to the experimental points.

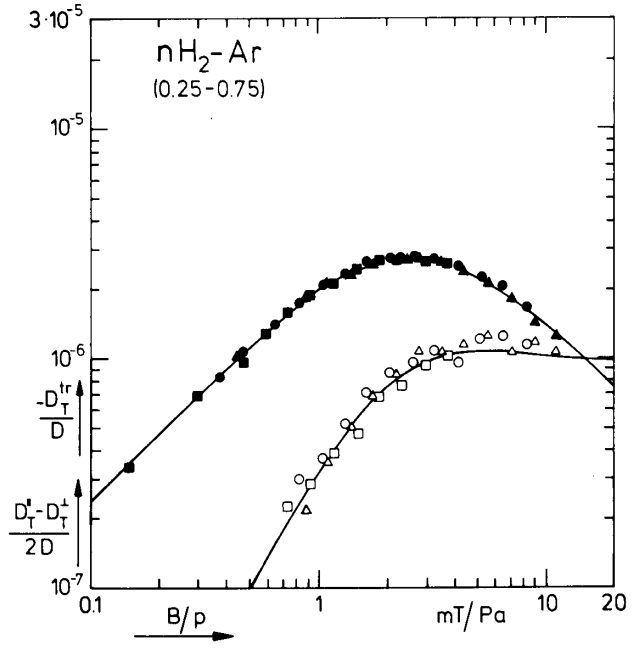

Fig. 16. $-D_T^{tr}/D$ and $(D_T^{\parallel} - D_T^{\perp})/2D$ versus B/p for nH_2–Ar ($x_{noblg\,gas} = 0.75$); ▲△ 177.2 Pa; ●○ 268.1 Pa; ■□ 532.9 Pa; —— theoretical curves of eqs. (11) fitted to the experimental points.

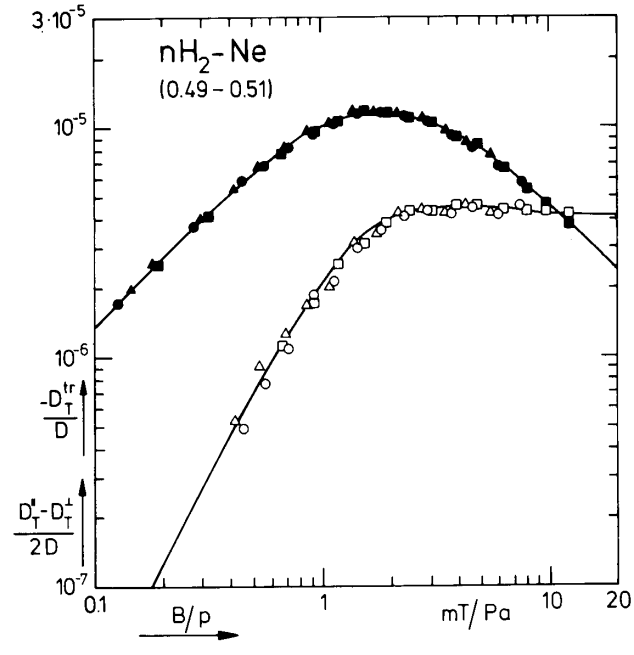

Fig. 17. $-D_T^{tr}/D$ and $(D_T^{\parallel} - D_T^{\perp})/2D$ versus B/p for nH_2–Ne ($x_{noble\,gas} = 0.51$); ■□ 179.1 Pa; ●○ 266.8 Pa; ▲△ 401.1 Pa; —— theoretical curves of eqs. (11) fitted to the experimental points.

$\mathcal{S}(\begin{smallmatrix}1010\\1001\end{smallmatrix}\,|\,{}^{A}_{A})_{AA}$, which is purely inelastic, are given[7,27]). It is seen from table I that both types of off-diagonal cross sections are small in comparison to the diagonal one, and can thus be neglected.

Using the expression for the field free diffusion coefficient in terms of effective cross sections

$$D = \frac{kT}{m_A} \frac{1}{n v_{AB} \mathcal{S}(\begin{smallmatrix}1000\\1000\end{smallmatrix}\,|\,{}^{A}_{A})_{AB}}, \tag{20}$$

it follows from eqs. (13), (14) and (15), that the magnetic field effects on thermal conductivity, diffusion and thermal diffusion are related by

$$|\Psi^{\mathrm{T}}_{pq}| = \sqrt{\frac{x_A x_B \lambda}{nkD}\, \Psi^{D}_{pq} \Psi^{\lambda}_{pq}}. \tag{21}$$

This relation is also valid when the off-diagonal cross sections in eqs. (13), (14) and (15) are retained[17]).

In the derivation of eqs. (11) the approximation was made, that the matrix elements $\langle [\boldsymbol{W}]^p_m [\boldsymbol{J}]^q_s \,|\, \mathcal{R} [\boldsymbol{W}]^p_{m'} [\boldsymbol{J}]^q_{s'} \rangle_0$ of the collision operator, $\mathcal{R}$, are proportional to $\delta_{mm'}\delta_{ss'}$. (Here $[\boldsymbol{W}]^p_m$ denotes the spherical m-component of a traceless symmetric irreducible tensor of rank p in $\boldsymbol{W}$.) This is called the "Spherical Approximation" since the above condition is strictly valid for a purely spherical potential. Thus the spherical approximation can be expected to work very well for molecules with a small nonsphericity of their interaction, e.g., H_2 and D_2, but it may be somewhat doubtful for molecules like N_2. If one defines, in the case of the $\boldsymbol{WJJ}$-polarization, totally irreducible lth-rank tensors $[[\boldsymbol{W}]^1[\boldsymbol{J}]^2]^l_m$ built up from $[\boldsymbol{W}]^1$ and $[\boldsymbol{J}]^2$, the collision operator becomes diagonal in l and m irrespective of the form of the potential because of rotational invariance. The matrix elements of $\mathcal{R}$ which govern the decay of $[[\boldsymbol{W}]^1[\boldsymbol{J}]^2]^l$-polarizations are represented by $\bar{\mathcal{S}}_l(\begin{smallmatrix}1200\\1200\end{smallmatrix}\,|\,{}^{A}_{A})_{Ak}$ ($l = 1,2$ or 3, $k = A$ or B) defined in ref. 28. The expressions for Ψ_{12} do not change. The field dependence of the transport coefficients, however, becomes complicated because the Liouville operator, which governs the free precessional motion of the molecules in the field, is not diagonal in l and m indices. The eqs. (11) now change into (see also refs. 7, 27, 28 and 29)

$$\begin{aligned}
\frac{\Delta D^{\perp}_{\mathrm{T}}}{D} &= -\Psi^{\mathrm{T}}_{12} \frac{10}{3} \frac{\bar{\xi}^2_{12}[\bar{\xi}^2_{12}(\frac{4}{5}a_2 + a_3 + \frac{1}{5}a_2a_3) - 1][\frac{4}{5}a_2 + a_3] + [\frac{9}{4} + \frac{5}{4}a_2 + a_3]}{[\bar{\xi}^2_{12}(\frac{4}{5}a_2 + a_3 + \frac{1}{5}a_2a_3) - 1]^2 + \bar{\xi}^2_{12}(\frac{3}{2} + \frac{5}{6}a_2 + \frac{2}{3}a_3)^2}, \\
\frac{\Delta D^{\parallel}_{\mathrm{T}}}{D} &= -2\Psi^{\mathrm{T}}_{12} \frac{a_2 \bar{\xi}^2_{12}}{1 + \bar{\xi}^2_{12}(\frac{2}{5}a_2a_3 + \frac{3}{5}a_2)}, \\
\frac{D^{\mathrm{u}}_{\mathrm{T}}(B)}{D} &= -\tfrac{5}{9}\Psi^{\mathrm{T}}_{12}\bar{\xi}_{12}\{(1 - \tfrac{1}{5}\bar{\xi}^2_{12}a_2a_3)(9 + 5a_2 + 4a_3)
\end{aligned} \tag{22}$$

$$- (5a_2 + 4a_3)[1 - \bar{\xi}_{12}^2(\tfrac{4}{5}a_2 + a_3 + \tfrac{1}{5}a_2a_3)]\}$$
$$\times \{[\bar{\xi}_{12}^2(\tfrac{4}{5}a_2 + a_3 + \tfrac{1}{5}a_2a_3) - 1]^2 + \bar{\xi}_{12}^2(\tfrac{3}{2} + \tfrac{5}{6}a_2 + \tfrac{2}{3}a_3)^2\}^{-1},$$

where

$$\bar{\xi}_{12} = \frac{g\mu_N kT}{\hbar}\{x_A v_{AA}\bar{\mathfrak{S}}_1(\begin{smallmatrix}1200\\1200\end{smallmatrix}\,|\,\begin{smallmatrix}A\\A\end{smallmatrix})_{AA} + x_B v_{AB}\bar{\mathfrak{S}}_1(\begin{smallmatrix}1200\\1200\end{smallmatrix}\,|\,\begin{smallmatrix}A\\A\end{smallmatrix})_{AB}\}^{-1}\frac{B}{p}$$

and

$$a_l = \frac{x_A v_{AA}\bar{\mathfrak{S}}_1(\begin{smallmatrix}1200\\1200\end{smallmatrix}\,|\,\begin{smallmatrix}A\\A\end{smallmatrix})_{AA} + x_B v_{AB}\bar{\mathfrak{S}}_1(\begin{smallmatrix}1200\\1200\end{smallmatrix}\,|\,\begin{smallmatrix}A\\A\end{smallmatrix})_{AB}}{x_A v_{AA}\bar{\mathfrak{S}}_l(\begin{smallmatrix}1200\\1200\end{smallmatrix}\,|\,\begin{smallmatrix}A\\A\end{smallmatrix})_{AA} + x_B v_{AB}\bar{\mathfrak{S}}_l(\begin{smallmatrix}1200\\1200\end{smallmatrix}\,|\,\begin{smallmatrix}A\\A\end{smallmatrix})_{AB}}, \quad l = 2, 3.$$

Similar equations hold for $\boldsymbol{\lambda}$ and $\boldsymbol{D}$, with the same field parameters $\bar{\xi}_{12}$, a_2 and a_3, but with other parameters governing the magnitudes (Ψ_{12}^{λ} and Ψ_{12}^{D}, respectively). In the spherical approximation $\bar{\mathfrak{S}}_1(\begin{smallmatrix}1200\\1200\end{smallmatrix}\,|\,\begin{smallmatrix}A\\A\end{smallmatrix})_{Ak} = \bar{\mathfrak{S}}_2(\begin{smallmatrix}1200\\1200\end{smallmatrix}\,|\,\begin{smallmatrix}A\\A\end{smallmatrix})_{Ak} = \bar{\mathfrak{S}}_3(\begin{smallmatrix}1200\\1200\end{smallmatrix}\,|\,\begin{smallmatrix}A\\A\end{smallmatrix})_{Ak} = \mathfrak{S}(\begin{smallmatrix}1200\\1200\end{smallmatrix}\,|\,\begin{smallmatrix}A\\A\end{smallmatrix})_{Ak}$, $a_2 = a_3 = 1$ and $\bar{\xi}_{12} = \xi_{12}$, so that eqs. (11) are recovered.

4. Description of the apparatus

The apparatus essentially consists of a long channel enclosed between two plates held at different temperatures, effective length $l = 1.48$ m, thickness $t = 6.0$ mm and width 6.0 mm. In order to fit such a long channel between the poles of a magnet a design as shown in fig. 3 is chosen. The design is in

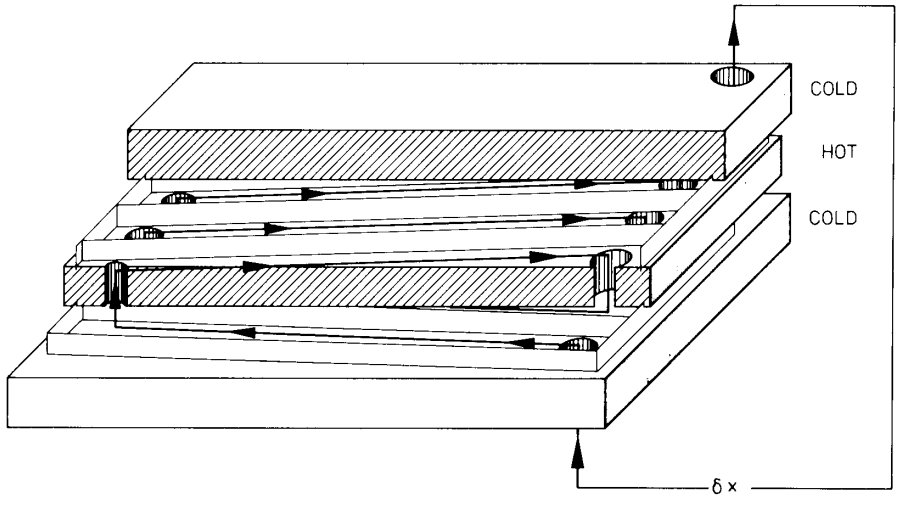

Fig. 3. Schematic diagram of the apparatus (note that the actual apparatus is turned over $\pi/4$).

essence similar to the apparatus of Hulsman et al.[30]) for the investigation of the thermomagnetic pressure difference. In our case, the channel consists of 20 sections of effective lengths of 74 mm connected by holes of 4 mm diameter. Thin brass foil (0.05 mm) soldered into the hot and cold plates is used to separate adjacent channel sections. Because of the "spiral" shape of the total channel the parts between the top and the middle plate make a small angle, δ, with the parts between the middle and the bottom plate. When for instance the magnetic field is perpendicular to the plane of drawing of fig. 3, the angles which the magnetic field makes with the different parts of the channel are $(\pi + \delta)/2$ and $(\pi - \delta)/2$. As can easily be verified using eq. (5), this will not give rise to additional effects. It only reduces the effective length of the channel (by a factor $\cos(\delta/2)$). This correction is negligibly small because $\delta = 0.038$ radians. Since the magnetic field direction can only be varied in the horizontal plane the apparatus is placed under an angle $\pi/4$ (see fig. 4). To guarantee temperature homogeneity the hot plate is heated by means of 8 heaters distributed throughout the plate. The cold plates are cooled by water from a thermostat and have temperature variations smaller than 5 mK. In all three plates temperature dependent resistors, NTC's, are mounted in order to measure the applied temperature difference, ΔT, typically 10 K. For temperature stabilization the apparatus is surrounded by a vacuum jacket. The concentration difference across the channel is measured by determining the difference in thermal conductivity of the gas. In order to attain high sensitivity the ends of the channel lead to two chambers in a thermally isolated, copper block (not shown in fig. 4), in which katharometer type thermistors (ITT P 15) are placed. By electrically heating these thermistors in a Wheatstone bridge circuit relative changes of the thermal conductivity as small as 2 ppm can be detected. This corresponds to concentration differences of the same amount for a typical system. To avoid effects of the magnetic field on the thermistors it proved to be necessary to place the copper block outside the magnetic field. The differences in thermal conductivity are calibrated in terms of concentration differences by observing the signal of the Wheatstone bridge when several calibrating mixtures of known composition are introduced into the apparatus. At the pressures used (about 100 to 300 Pa) the mean free path in most gases is of the order of the dimensions of the thermistors (approximately 0.2 mm). This means that the heat transport becomes pressure dependent (Knudsen effect). As a consequence, for every pressure run a calibration had to be performed at that particular pressure, and the pressures of different calibration mixtures had to be the same within 1 in 10^3. To this end a high accuracy manometer (Datametrics Barocel 10 T, type 570 D) was used.

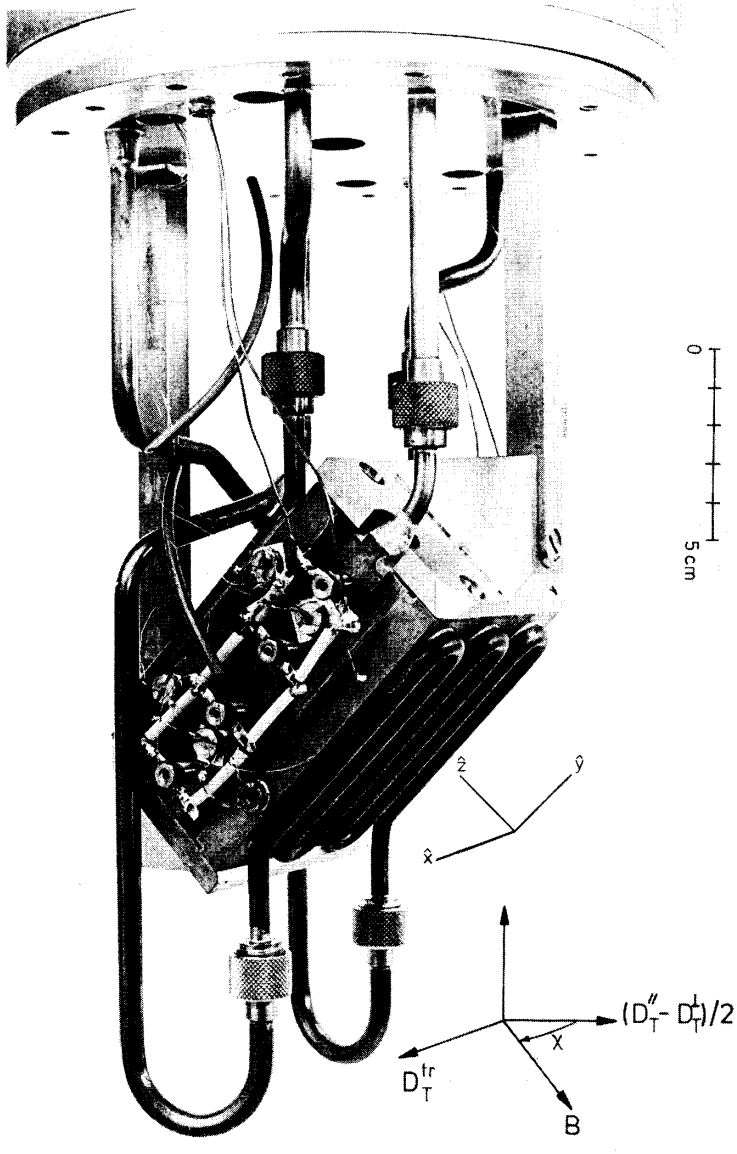

Fig. 4. Photograph of the apparatus.

5. Corrections

Using eqs. (9) and (10) D_T^{tr}/D and $(D_T^{\#} - D_T^{\perp})/2D$ are calculated from the measured concentration differences. In fig. 5 a double logarithmic plot is made of $(D_T^{tr}/D)_{meas}$ and $((D_T^{\#} - D_T^{\perp})/2D)_{meas}$ versus B/p for an equimolar N_2–Ar

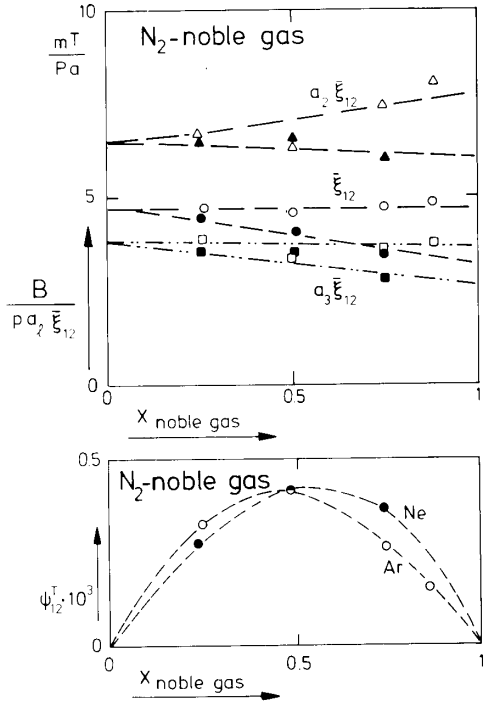

Fig. 9. a $B/pa_i\bar{\xi}_{12}$ versus noble gas mole fraction; ○△□ N_2–Ar; ●▲■ N_2–Ne. b. Ψ^T_{12} versus noble gas mole fraction; ○ N_2–Ar; ● N_2–Ne. The experimental results are obtained by fitting $\boldsymbol{D}_T(\boldsymbol{B})$ measurements to the theoretical curves of eqs. (22).

TABLE IV
Experimental results

Gas	$x_{\text{noble gas}}$	$\Psi^T_{12} \times 10^6$	$B/p\xi_{12}$ (mT/Pa)	$\Psi^T_{11} \times 10^6$	$B/p\xi_{11}$ (mT/Pa)	$\Psi^\lambda_{12} \times 10^3$	λ (W/Km)
N_2–Ar	0.2545	292	4.87	− 76	2.90	2.98 [15])	0.0231 [15])
	0.4986	373	4.72	−109	3.22	1.91	0.0214
	0.7475	227	4.94	− 83	3.02	0.90	0.0196
	0.8751	135	5.10	− 50	2.87	0.42	0.0186
N_2–Ne	0.2491	226	4.44	− 46	1.85	3.41 [15])	0.0294 [15])
	0.5018	378	4.04	−104	3.11	2.50	0.0344
	0.7498	329	3.63	−101	4.02	1.39	0.0401
N_2–He	0.2502	141	4.32			2.56 [15])	0.0393 [15])
	0.5002	248	3.52			1.43	0.0580
	0.7485	240	2.71			0.65	0.0880
HD–Ar	0.1251	−26.6	2.32			0.447 [15])	0.1549 [15])
	0.2531	−29.6	2.36			0.297	0.1014
	0.4467	−21.7	2.58			0.155	0.0633
	0.7496	− 9.0	2.67			0.058	0.0374

TABLE IV (*continued*)
Experimental results

Gas	$x_{\text{noble gas}}$	$\Psi_{12}^{T} \times 10^{6}$	$B/p\xi_{12}$ (mT/Pa)	$\Psi_{11}^{T} \times 10^{6}$	$B/p\xi_{11}$ (mT/Pa)	$\Psi_{12}^{\lambda} \times 10^{3}$	λ (W/Km)
HD–Ne	0.2502	19.6	2.54	small		0.387 [15])	0.1210 [15])
	0.5016	25.8	2.56			0.207	0.0909
	0.7496	18.0	2.56			0.093	0.0668
HD–He	0.2602	37.9	2.32	small		0.467 [15])	0.1545 [15])
	0.5027	38.9	2.15	small		0.315	0.1535
	0.7490	36.0	2.08	small		0.158	0.1521
pH_2	0					0.037 [22])	
pH_2–Ar	0.2495	3.92	2.69				0.1162 [35])
	0.5015	3.87	3.16				0.0712
	0.7501	2.02	3.65				0.0409
nH_2	0					0.030 [22])	
nH_2–Ar	0.2461	3.09	2.90	small			0.1169 [35])
	0.5011	4.04	3.42				0.0713
	0.7482	2.37	4.06				0.0411
nH_2–Ne	0.2484	6.52	2.52				0.1360 [36])
	0.5069	8.36	2.93				0.0970
	0.7523	6.53	3.38				0.0685
nH_2–He	0.2493	4.77	2.32				0.1724 [35])
	0.5003	7.39	2.32				0.1613
	0.7484	5.88	2.32				0.1545
nD_2	0					0.037 [22])	
nD_2–Ar	0.2493	3.24	3.77	small			0.0852 [35])
	0.5024	3.14	4.75				0.0542
	0.7497	1.40	5.48				0.0335
nD_2–Ne	0.2503	9.66	3.29				0.1044 [37])
	0.5001	12.9	3.53				0.0820
	0.7505	7.92	3.90				0.0642
nD_2–He	0.2500	9.8	2.90	−1.8	0.89		0.1347 [35])
	0.5015	12.2	2.81	−3.3	0.85		0.1386
	0.7500	8.4	2.81	−4.7	0.98		0.1445
	0.8650	6.6	2.72	−4.8	1.01		0.1484

small: $|\Psi_{11}^{T}/\Psi_{12}^{T}| < 0.10$

be discussed in the following sections. It is noted that in all cases where ***WJ***-polarizations are found in the thermal diffusion measurements Ψ_{11}^{T} and Ψ_{12}^{T} have opposite signs.

PHYSICA A VOL 96 NO 1 + 2 DEC 4

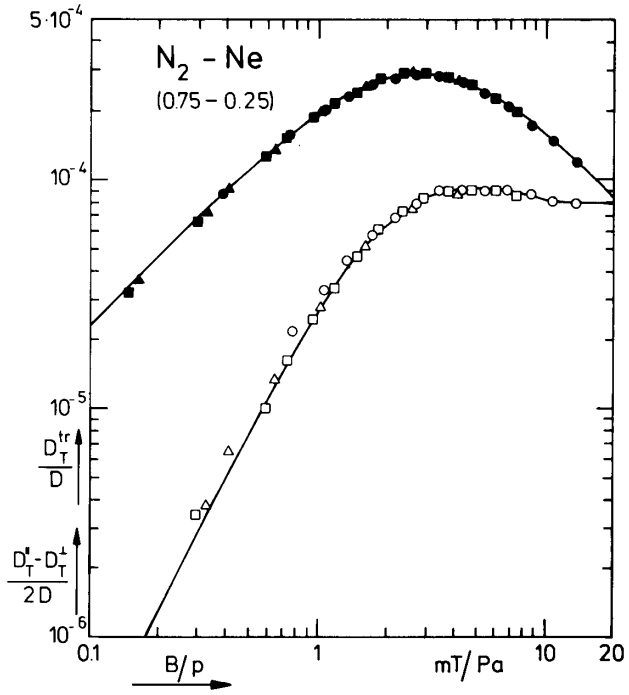

Fig. 10. D_T^{tr}/D and $(D_T^{\parallel} - D_T^{\perp})/2D$ versus B/p for N_2–Ne ($x_{\text{noble gas}} = 0.25$); ●○ 164.0 Pa; ■□ 265.5 Pa; ▲△ 482.5 Pa; —— theoretical curves of eqs. (11) fitted to the experimental points.

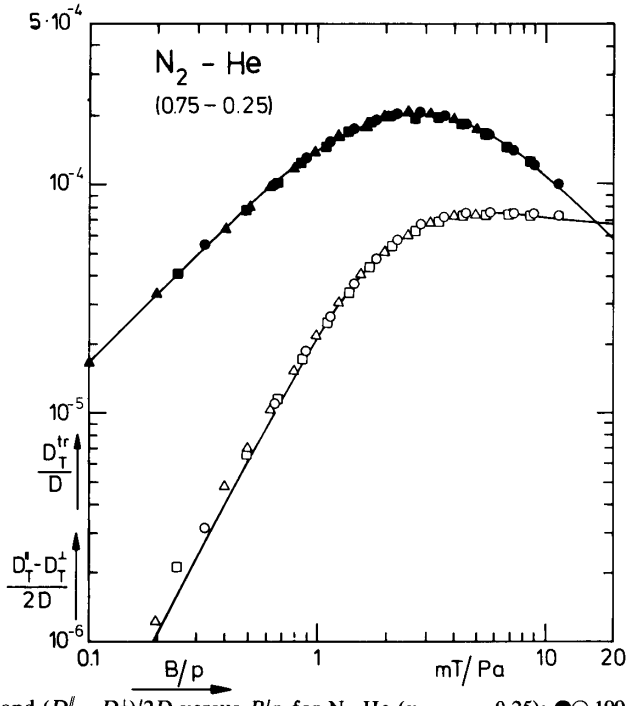

Fig. 11. D_T^{tr}/D and $(D_T^{\parallel} - D_T^{\perp})/2D$ versus B/p for N_2–He ($x_{\text{noble gas}} = 0.25$); ●○ 199 Pa; ■□ 263 Pa; ▲△ 405 Pa; —— theoretical curves of eqs. (11) fitted to the experimental points.

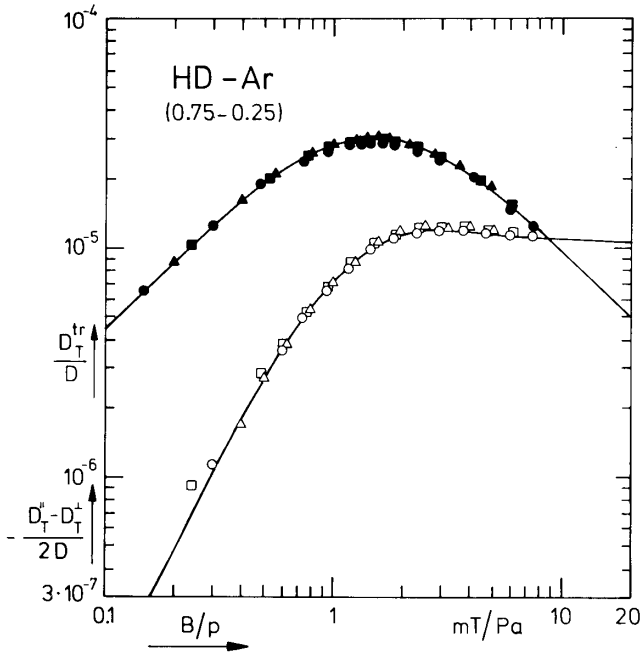

Fig. 12. D_T^{tr}/D and $(D_T^{\perp} - D_T^{\parallel})/2D$ versus B/p for HD–Ar ($x_{\text{noble gas}} = 0.25$); ●○ 266.9 Pa; ■□ 329.7 Pa; ▲△ 398.0 Pa; —— theoretical curves of eqs. (11) fitted to the experimental points.

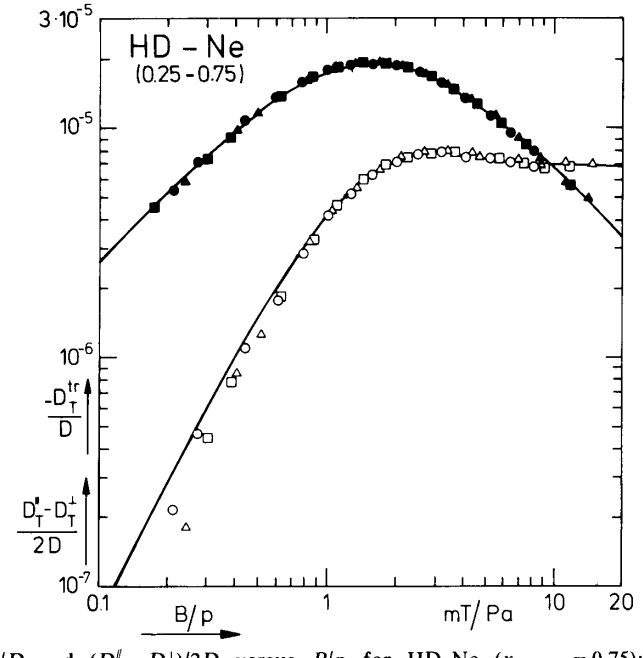

Fig. 13. $-D_T^{tr}/D$ and $(D_T^{\parallel} - D_T^{\perp})/2D$ versus B/p for HD–Ne ($x_{\text{noble gas}} = 0.75$); ▲△ 141.1 Pa; ■□ 190.5 Pa; ●○ 269.3 Pa; —— theoretical curves of eqs. (11) fitted to the experimental points.

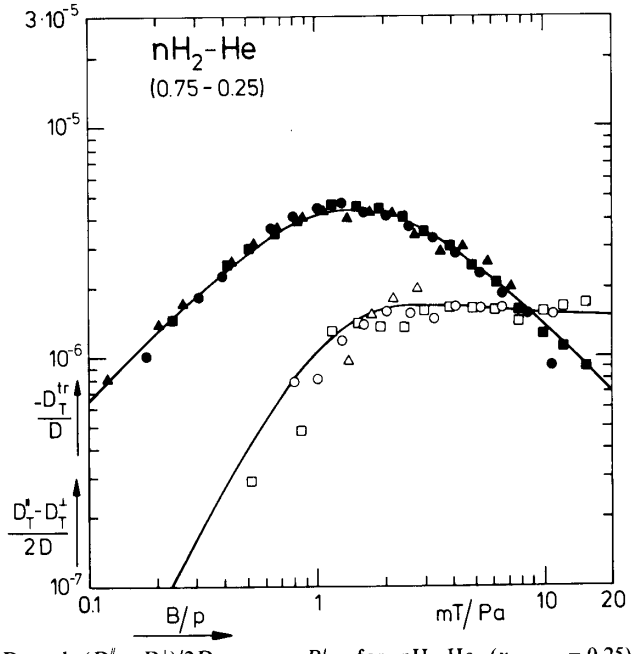

Fig. 18. $-D_T^{tr}/D$ and $(D_T^{\parallel} - D_T^{\perp})/2D$ versus B/p for nH_2–He ($x_{\text{noble gas}} = 0.25$); ■□ 143.0 Pa; ●○ 188.5 Pa; ▲△ 283.0 Pa; —— theoretical curves of eqs. (11) fitted to the experimental points.

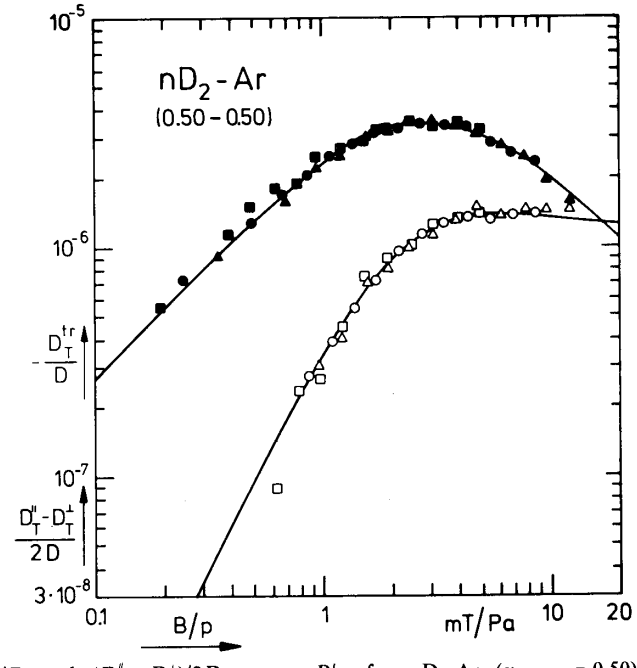

Fig. 19. $-D_T^{tr}/D$ and $(D_T^{\parallel} - D_T^{\perp})/2D$ versus B/p for nD_2–Ar ($x_{\text{noble gas}} = 0.50$); ▲△ 181.0 Pa; ●○ 257.2 Pa; ■□ 404.0 Pa; —— theoretical curves of eqs. (11) fitted to the experimental points.

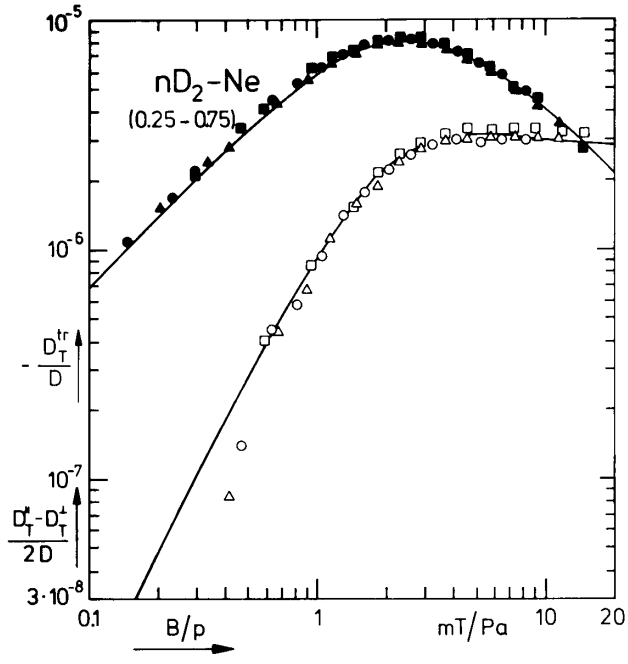

Fig. 20. $-D_T^{tr}/D$ and $(D_T^{\parallel} - D_T^{\perp})/2D$ versus B/p for nD_2–Ne ($x_{\text{noble gas}} = 0.75$). ■□ 133.5 Pa; ▲△ 189.1 Pa; ●○ 267.9 Pa; —— theoretical curves of eqs. (11) fitted to the experimental points.

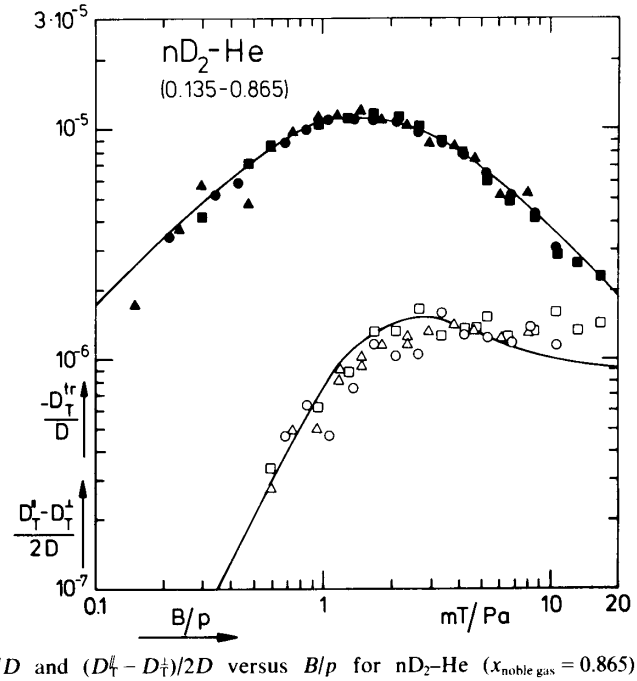

Fig. 21. $-D_T^{tr}/D$ and $(D_T^{\parallel} - D_T^{\perp})/2D$ versus B/p for nD_2–He ($x_{\text{noble gas}} = 0.865$); ■□ 134.3 Pa; ●○ 187.0 Pa; ▲△ 267.2 Pa; —— theoretical curves of eqs. (11) fitted to the experimental points.

7. The position on the B/p-axis

In this section we relate the quantities $B/p\xi_{12}$ and $B/p\xi_{11}$, which determine the position on the B/p-axis of the thermal diffusion effects, to theoretical expressions involving effective cross sections. Rewriting eq. (12), gives

$$\frac{B}{p\xi_{pq}} = \frac{\hbar v_{AA}}{g\mu_N kT}\left[(1-x_B)\Im\left(\begin{smallmatrix}pq00\\pq00\end{smallmatrix}\middle|\begin{smallmatrix}A\\A\end{smallmatrix}\right)_{AA} + x_B\sqrt{\frac{m_A+m_B}{2m_B}}\,\Im\left(\begin{smallmatrix}pq00\\pq00\end{smallmatrix}\middle|\begin{smallmatrix}A\\A\end{smallmatrix}\right)_{AB}\right], \tag{24}$$

with $pq = 11$ or 12. In fig. 22 $B/p\xi_{12}$ and $B/p\xi_{11}$ are plotted versus noble gas

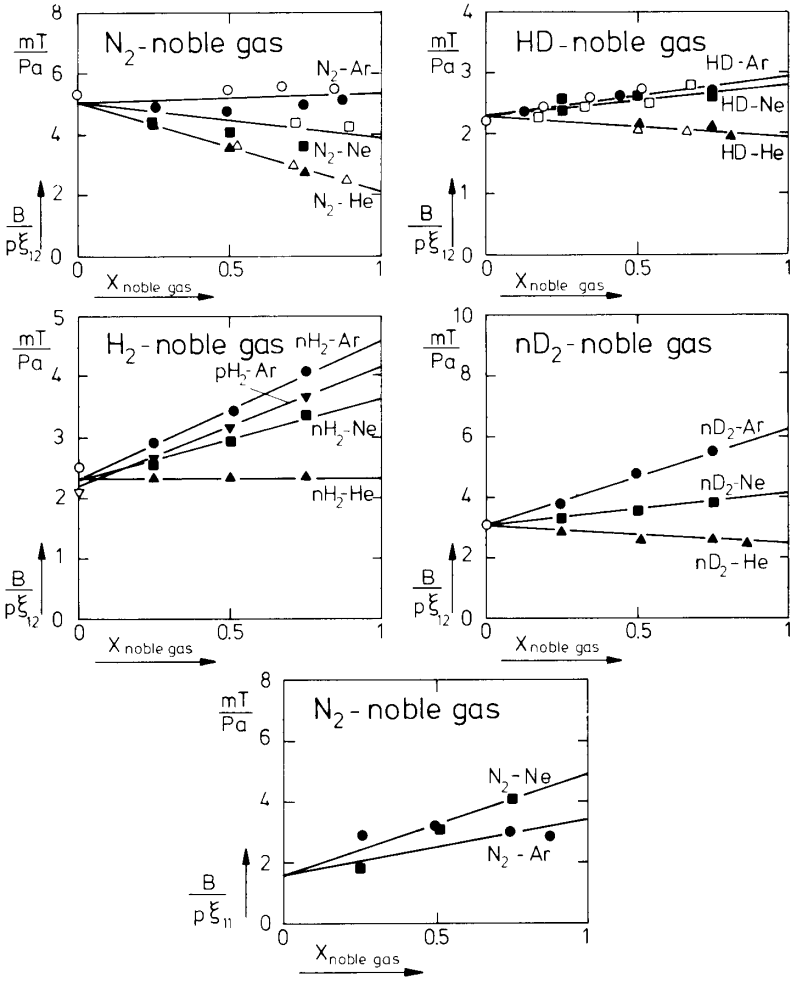

Fig. 22. $B/p\xi_{12}$ versus the mole fraction of the noble gas for N_2, HD, H_2 and D_2–noble gas mixtures and $B/p\xi_{11}$ versus the mole fraction of the noble gas for N_2–Ar and N_2 – Ne; ●■▲ from $D_T(B)$; ○□△ from $\lambda(B)$ (refs. 15 and 22).

mole fraction, x_B. It is clear from those graphs that $B/p\xi_{12}$ does depend linearly on the concentration in agreement with eq. (24). As pointed out before the position on the B/p-axis should be the same for the thermal conductivity and the thermal diffusion measurements. The experimental data for $B/p\xi_{12}$ as obtained from the measurements of the thermal conductivity of N_2–noble gas and HD–noble gas mixtures of ref. 15 and those of pH_2, nH_2 and nD_2 of ref. 22 are also plotted in the graphs. The agreement between the results of the $\boldsymbol{\lambda}$ and $\boldsymbol{D}_T$ experiments is quite good over the entire concentration range, except for N_2–Ar and N_2–Ne where small deviations occur. These discrepancies are probably due to the fact that for thermal conductivity Ψ^{λ}_{12} and $B/p\xi_{12}$ can be fairly accurately determined with a 2 parameter fit, while for thermal diffusion a 4 parameter fit is needed, making the data less accurate. The $B/p\xi_{12}$ results for a polyatomic gas mixture with different noble gases should extrapolate to the same value at $x_{\text{noble gas}} = 0$, since then only quantities of the polyatomic gas are relevant. This is indeed observed within the limits of the experimental accuracy. The straight lines through the points of fig. 22 are drawn in such a way that they intersect at $x_{\text{noble gas}} = 0$. Extrapolations to $x_{\text{noble gas}} = 0$ and 1 yield two cross sections, $\mathfrak{S}(\begin{smallmatrix}1200\\1200\end{smallmatrix}\,|\,\begin{smallmatrix}A\\A\end{smallmatrix})_{AA}$ and $\mathfrak{S}(\begin{smallmatrix}1200\\1200\end{smallmatrix}\,|\,\begin{smallmatrix}A\\A\end{smallmatrix})_{AB}$, respectively. These effective cross sections are listed in table V, and will be further discussed in section 10.

For the systems N_2–Ar and N_2–Ne data on the position on the B/p-axis of the ***WJ***-polarization are also obtained (last graph in fig. 22). The two straight lines are fitted to the experimental points according to eq. (24) with intersection at $x_{\text{noble gas}} = 0$. Here the differences between theory and experiment are quite large, but this is easily explained by the fact that when $\Psi^{T}_{11}/\Psi^{T}_{12}$ is smaller than about 0.5, the position on the B/p-axis of D^{tr}_T/D and $(D^{\parallel}_T - D^{\perp}_T)/2D$ is largely defined by $B/p\xi_{12}$ and is not very sensitive to $B/p\xi_{11}$. The values of $B/p\xi_{11}$ cannot be accurately determined in this way and cross sections obtained from extrapolations to $x_{\text{noble gas}} = 0$ and 1, will be correct within, say, a factor of 2. In principle, one could also obtain values for $B/p\xi_{11}$ from the thermal conductivity measurements. However, from the measurements on $\lambda^{\perp}$ and $\lambda^{\parallel}$ of N_2–Ar and N_2–Ne no consistent data on $B/p\xi_{11}$ could be extracted mainly because the contributions from the ***WJ***-polarization were too small[7,15]). The values of $\mathfrak{S}(\begin{smallmatrix}1100\\1100\end{smallmatrix}\,|\,\begin{smallmatrix}A\\A\end{smallmatrix})_{kl}$ for N_2–Ar and N_2–Ne are listed in table V.

8. The magnitude of the effect and determination of $\mathfrak{S}(\begin{smallmatrix}1000\\pq00\end{smallmatrix}\,|\,\begin{smallmatrix}A\\A\end{smallmatrix})_{AB}$

For the mixtures N_2, HD, nH_2 and nD_2 with Ar, Ne and He and the system pH_2–Ar, Ψ^{T}_{12} is plotted versus noble gas mole fraction in fig. 23, where Ψ^{T}_{11} for the systems N_2–Ar and N_2–Ne is also given. The results are summarized in

TABLE V
Effective cross sections (T = 300 K) in 10^{-20} m^2

	$\Im(^{1200}_{1200}\mid ^{A}_{A})_{kl}$	$\Im(^{0200}_{0200}\mid ^{A}_{A})_{kl}$	$\Im(^{1010}_{1200}\mid ^{A}_{A})_{kl}$	$\lvert\Im(^{1000}_{1200}\mid ^{A}_{A})_{AB}\rvert$	$\Im(^{0200}_{2000}\mid ^{A}_{A})_{kl}$	$\Im(^{1001}_{1200}\mid ^{A}_{A})_{AA}$	$\Im(^{1000}_{1100}\mid ^{A}_{A})_{AB}$	$\Im(^{1100}_{1100}\mid ^{A}_{A})_{kl}$
N_2	40.9	23.7 [16])	−0.67 [16])		1.49 [16])	4.39 [7])		16
N_2–Ar	46.7	24 [16])	−5.4	0.66	0.98 [16])		0.34	26
N_2–Ne	28.5	15 [16])	+1.4	0.37	0.54 [16])		0.18	39
N_2–He	8.7	5.6 [16])	−0.04	0.121	0.081 [16])			
HD	14.5	2.26 [16])	−0.12 [16])		0.282 [16])	0.67 [7])		
HD–Ar	25.6	4.9 [16])	−0.086	0.13	0.59 [16])			
HD–Ne	23.6	3.3 [16])	−0.33	0.092	0.32 [16])			
HD–He	13.3	2.1 [16])	−1.0	0.077	0.14 [16])			
pH_2	15.4	0.50 [45])	−0.0088 [45])		0.020 [45])	0.21 [7])		
pH_2–Ar	39.6			0.065				
nH_2	16.0	0.52 [45])	−0.0060 [45])		0.013 [45])	0.21 [7])		
nH_2–Ar	44.3			0.047				
nH_2–Ne	34.1			0.097				
nH_2–He	18.5			0.052				
nD_2	15.2	0.89 [45])	−0.0121 [45])		0.027 [45])	0.21 [7])		
nD_2–Ar	41.8			0.052				
nD_2–Ne	26.5			0.11				
nD_2–He	12.9			0.087				

$kl = AA$ or AB

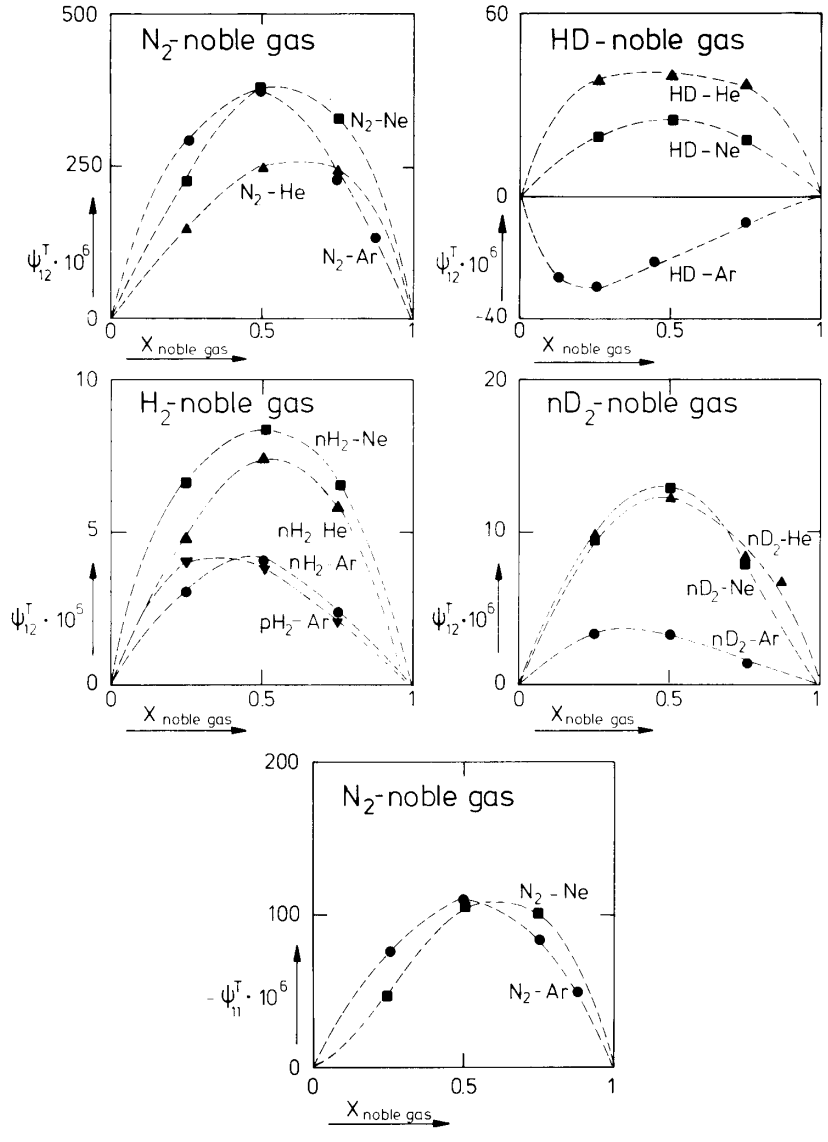

Fig. 23. Ψ^T_{12} of N_2, HD, H_2, D_2–noble gas mixtures and Ψ^T_{11} of N_2–Ne and N_2–Ar versus the mole fraction of the noble gas.

table IV. Theoretically, as is evident from eq. (14), Ψ^T_{pq} has a trivial $x_B(1-x_B)$ concentration dependence. Fig. 23 shows that this concentration dependence is dominant. The magnitude of the thermal diffusion change is such that for the N_2–noble gas systems Ψ^T_{12} is about 10^{-4}, for the HD–noble gas systems about 10^{-5}, and for H_2 and D_2–noble gas systems only 10^{-6}. In all cases the

corresponding value of Ψ^{λ}_{12}, the magnitude of the thermal conductivity change, is an order of magnitude larger. The sign of Ψ^{T}_{12} is always found to be positive except for the system HD–Ar. The values found for Ψ^{T}_{11} are negative. The physical significance of a positive Ψ^{T}_{12} is that in the configuration of fig. 1a the concentration gradient of the polyatomic molecule is pointed to the right when the g-factor is negative (N_2–Ar, N_2–Ne, N_2–He).

As was already mentioned in section 5 the raw data for the system D_2–He show a strange pressure dependence at higher noble gas concentration. It is not clear, whether this may be partially responsible for the high ratio between $D^{\perp}_{T}/D$ and $(D^{\parallel}_{T} - D^{\perp}_{T})/2D$. If one tries to interpret this ratio with the use of the extra ***WJ***-polarization the agreement between theoretical and experimental curves is not satisfactory (see fig. 21). For this reason the values obtained for the parameters of the ***WJ***-polarization for this system have not been further analyzed. Abandoning the spherical approximation and then fitting the experimental results with the formulas (22), might yield a better agreement between theory and experiment. However, deviations from the spherical approximation are not to be expected when the nonsphericity is as small as for D_2.

Rearranging eqs. (15), (20) and (21) a relation between Ψ^{T}_{pq}, Ψ^{λ}_{pq} and the production cross section for the diffusion, $\mathcal{S}(^{1000}_{pq00}\,|\,^{A}_{A})_{AB}$, is derived to be:

$$|\mathcal{S}(^{1000}_{pq00}\,|\,^{A}_{A})_{AB}| = |\Psi^{T}_{pq}|\left[\frac{1}{\Psi^{\lambda}_{pq}\lambda}\frac{k^2T}{m_A}\{x_A v_{AA}\mathcal{S}(^{pq00}_{pq00}\,|\,^{A}_{A})_{AA} + x_B v_{AB}\mathcal{S}(^{pq00}_{pq00}\,|\,^{A}_{A})_{AB}\}\frac{\delta_{p1}\delta_{q2}+1}{x_A x_B^2 v_{AB}^2}\right]^{1/2}. \tag{25}$$

For the N_2–noble gas and HD–noble gas systems Ψ^{λ}_{12} and λ have been measured as a function of the concentration by Heemskerk et al.[15]). Using these data and the values for $\mathcal{S}(^{1200}_{1200}\,|\,^{A}_{A})_{AA}$ and $\mathcal{S}(^{1200}_{1200}\,|\,^{A}_{A})_{AB}$ (see section 7), the production cross section $\mathcal{S}(^{1200}_{1200}\,|\,^{A}_{A})_{AB}$ can be calculated for each concentration at which Ψ^{T}_{12} is known. The results are demonstrated in figs. 24 and 25. Since cross sections do not depend on the concentration straight, horizontal lines should be acquired. For the N_2–noble gas systems and HD–He this is indeed found. For HD–Ar and HD–Ne the values of $\mathcal{S}(^{1000}_{1200}\,|\,^{A}_{A})_{AB}$ obtained at different concentrations are not the same. These differences can be partially explained by the inaccuracies in the experimental quantities used in the calculation, but might also be due to the fact that in eq. (15) the off-diagonal cross sections have been neglected with respect to diagonal cross sections. If this approximation (treated in section 3) is not justified other production cross sections, like $\mathcal{S}(^{1001}_{1200}\,|\,^{A}_{A})$ and $\mathcal{S}(^{1010}_{1200}\,|\,^{B}_{A})$, play a role in the influence of an external field on the diffusion, and the concentration dependence of the effect will be more complicated than given in eq. (15).

To calculate $\mathcal{S}(^{1000}_{1100}\,|\,^{A}_{A})_{AB}$ the above procedure is followed for the data on Ψ^{T}_{11}, Ψ^{λ}_{11} in the case of N_2–Ar and N_2–Ne. The results are given in fig. 26. The average values of $\mathcal{S}(^{1000}_{1200}\,|\,^{A}_{A})_{AB}$ and $\mathcal{S}(^{1000}_{1100}\,|\,^{A}_{A})_{AB}$ of the N_2–noble gas and HD–noble gas systems are listed in table V. It must be emphasized that no statement can be made on the sign of $\mathcal{S}(^{1000}_{pq00}\,|\,^{A}_{A})_{AB}$ on the basis of experimental data alone. Model calculations[33,34]) show that $(\sqrt{(C^{A}_{rot}/k)}A - \sqrt{(5/2)}B)$ appearing in eq. (14) should be positive, which means that Ψ^{T}_{12} and $\mathcal{S}(^{1000}_{1200}\,|\,^{A}_{A})_{AB}$ have the same sign.

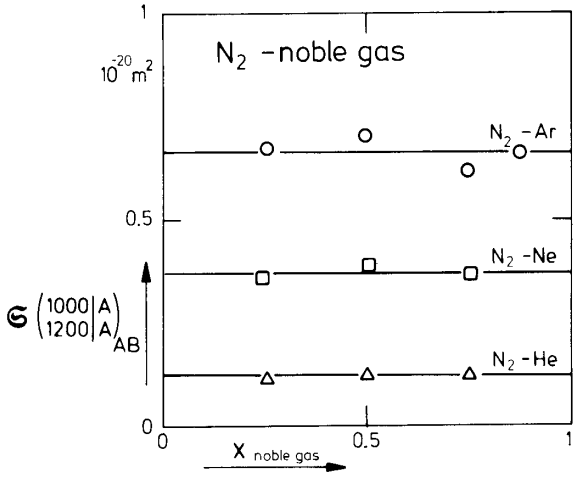

Fig. 24. The absolute value of $\mathcal{S}(^{1000}_{1200}\,|\,^{A}_{A})_{AB}$ for N_2–Noble gas systems as determined from measurements at various noble gas mole fractions.

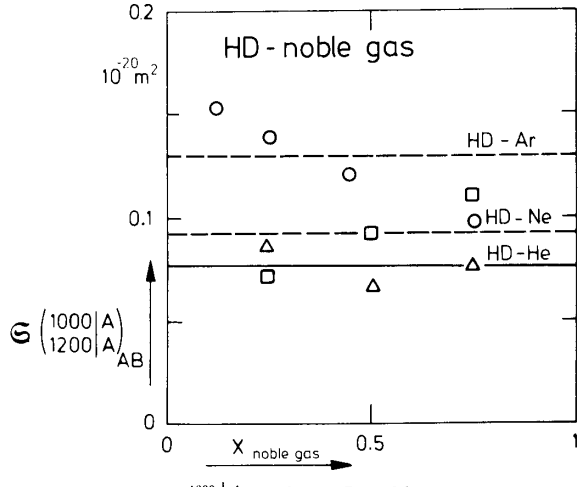

Fig. 25. The absolute value of $\mathcal{S}(^{1000}_{1200}\,|\,^{A}_{A})_{AB}$ for HD–noble gas systems as determined from measurements at various noble gas mole fractions; ○ HD–Ar; □ HD–Ne; △ HD–He.

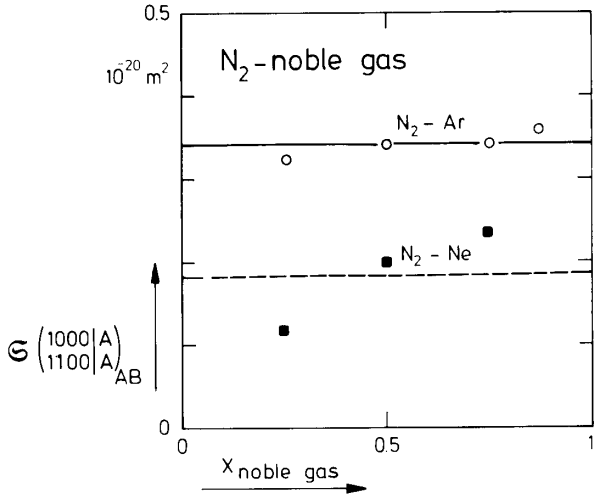

Fig. 26. The absolute value of $\mathfrak{S}(^{1000}_{1100}\,|\,^{A}_{A})_{AB}$ for N_2–Ar and N_2–Ne as determined from measurements at various noble gas mole fractions.

In the case of nH_2–noble gas, pH_2–Ar and nD_2–noble gas systems there are no data available for the concentration dependence of the field effect on the thermal conductivity. Only data for the pure gases nH_2, pH_2 and nD_2 are available from measurements of Hermans et al.[22]). The data handling of the thermal diffusion measurements of systems where only Ψ^{λ}_{12} ($x_{\text{noble gas}} = 0$) is

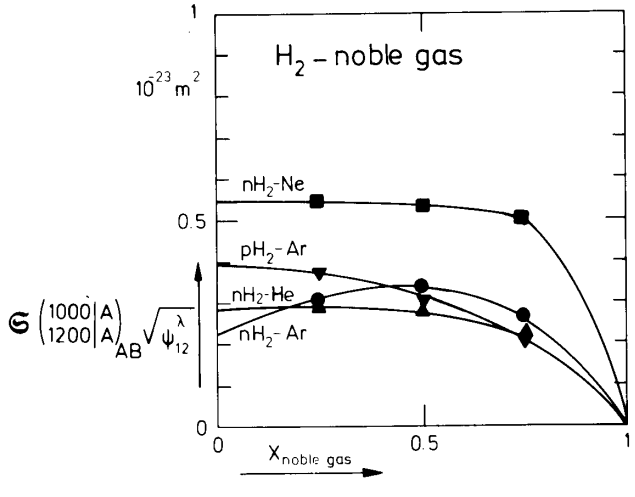

Fig. 27. The absolute value of $\mathfrak{S}(^{1000}_{1200}\,|\,^{A}_{A})_{AB}\sqrt{\Psi^{\lambda}_{12}}$ for nH_2–noble gas systems and pH_2–Ar as calculated from measurements at various noble gas mole fractions (eq. (26)).

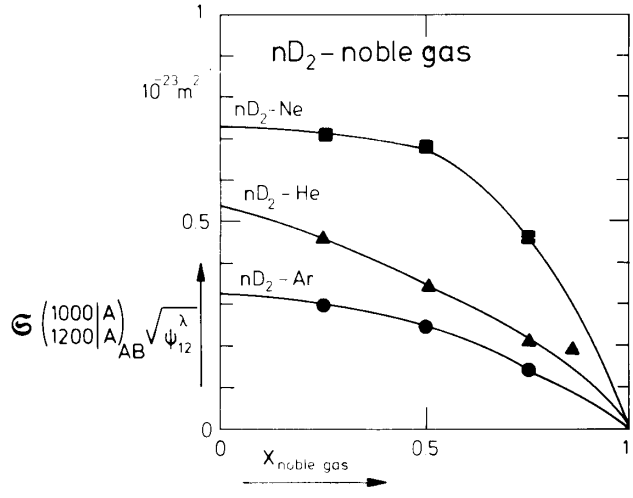

Fig. 28. The absolute value of $\mathfrak{S}(^{1000}_{1200}\,|\,^{A}_{A})_{AB}\sqrt{\Psi^{\lambda}_{12}}$ for nD_2–noble gas systems as calculated from measurements at various noble gas mole fractions (eq. (26)).

known, is as follows. A rearrangement of eq. (25) shows that with the data at hand $|\mathfrak{S}(^{1000}_{1200}\,|\,^{A}_{A})_{AB}|\sqrt{\Psi^{\lambda}_{12}}$ can be calculated according to

$$|\mathfrak{S}(^{1000}_{1200}\,|\,^{A}_{A})_{AB}|\sqrt{\Psi^{\lambda}_{12}} = |\Psi^{T}_{12}|\left[\frac{1}{\lambda}\frac{2k^2T}{m_A}\frac{1}{x_a x_B^2 v_{AB}^2}(x_A v_{AA}\mathfrak{S}(^{1200}_{1200}\,|\,^{A}_{A})_{AA} + x_B v_{AB}\mathfrak{S}(^{1200}_{1200}\,|\,^{A}_{A})_{AB})\right]^{1/2}. \tag{26}$$

Using the values for Ψ^{T}_{12}, λ and $B/p\xi_{12}$ listed in table IV, the results of such a calculation are given in fig. 27 for nH_2–noble gas and pH_2–Ar and in fig. 28 for the nD_2–noble gas systems. The data for $\lambda(x)$ are taken from the literature: for H_2–Ar, H_2–He, D_2–Ar and D_2–He from ref. 35, for H_2–Ne from ref. 36 and for D_2–Ne from ref. 37. The intercepts of the smoothed curves drawn through the points of figs. 27 and 28 together with values of Ψ^{λ}_{12} ($x_{\text{noble gas}} = 0$) from ref. 22 yield values for $|\mathfrak{S}(^{1000}_{1200}\,|\,^{A}_{A})_{AB}|$, which are listed in table V. Obviously this method is less accurate than the one used for the N_2–noble gas and HD–noble gas systems.

9. The field free diffusion coefficient

In sections 10 and 11 the cross section $\mathfrak{S}(^{1000}_{1000}\,|\,^{A}_{A})_{AB}$ will be needed. Values for this cross section can be obtained from literature on field free diffusion coefficients with the help of formula (20). Values of D at room temperature

and atmospheric pressure are taken from ref. 38 for the N_2–noble gas mixtures and H_2–noble gas mixtures, from ref. 39 for D_2–He and D_2–Ar, from ref. 40 for D_2–Ne, from ref. 41 for HD–He and from ref. 42 for HD–Ar (see table VI). For HD–Ne no literature value of D is found. Because $\mathcal{S}(^{1000}_{1000}\,|\,^{A}_{A})_{AB}$ is about the same for the three hydrogen isotopes H_2, ND, and D_2 with Ar and this also holds for the three hydrogen isotopes with He, the average of the values of $\mathcal{S}(^{1000}_{1000}\,|\,^{A}_{A})_{AB}$ for H_2–Ne and D_2–Ne is taken for the cross section for HD–NE (21×10^{-20} m^2). With this the predicted value for the diffusion coefficient at atmospheric pressure is estimated to be 9.6×10^{-5} m^2/s.

10. Discussion of the cross sections $\mathcal{S}(^{pq00}_{pq00}\,|\,^{A}_{A})_{AA}$, $\mathcal{S}(^{pq00}_{pq00}\,|\,^{A}_{A})_{AB}$, $\mathcal{S}(^{1000}_{1000}\,|\,^{A}_{A})_{AB}$ and $\mathcal{S}(^{1000}_{pq00}\,|\,^{A}_{A})_{AB}$

This section contains a discussion of some trends in the behavior of the various effective cross sections which have been obtained. First of all, let us make some general statements about effective cross sections. Most effective cross sections that describe the decay of a polarization, like $\mathcal{S}(^{1010}_{1010}\,|\,^{A}_{A})_{AA}$ and $\mathcal{S}(^{1200}_{1200}\,|\,^{A}_{A})_{AA}$, have energetically elastic contributions (no energy exchange

TABLE VI

Data concerning field free diffusion and the influence of an external field on the diffusion

	D (cm^2/s*)	$\mathcal{S}(^{1000}_{1000}\,|\,^{A}_{A})_{kl}$ (10^{-20} m^2)	$\dfrac{\mathcal{S}^{(0)}(^{1000}_{1000}\,|\,^{A}_{A})_{AB}}{\mathcal{S}(^{1000}_{1000}\,|\,^{A}_{A})_{AB}}$	$\Psi^{D}_{12} \times 10^6$ $x_{\text{noble gas}} = \frac{1}{2}$
N_2		26.3		
N_2–Ar	0.197 [38])	27.0	1.10	100
N_2–Ne	0.328 [38])	13.7	1.11	81
N_2–He	0.722 [38])	3.40	1.12	79
HD		14.1		
HD–Ar	0.701 [42])	29.1	1.17	5.0
HD–Ne	(0.97)	(21)	1.10	5.1
HD–He	1.391 [41])	11.5	1.11	6.5
pH_2–Ar	(0.822)	(30.7)	(1.13)	1.1
nH_2		13.9		
nH_2–Ar	0.822 [38])	30.7	1.13	0.54
nH_2–Ne	1.154 [38])	21.5	1.12	3.9
nH_2–He	1.542 [38])	13.7	1.09	2.7
nD_2		14.2		
nD_2–Ar	0.575 [39])	30.4	1.10	0.77
nD_2–Ne	0.832 [40])	20.1	1.10	6.5
nD_2–He	1.25 [39])	10.3	1.09	14

* Diffusion coefficients are given for $p \simeq 1.013 \times 10^5$ Pa and $T = 300$ K.

between translational degrees of freedom and rotational degrees of freedom). Exceptions are, e.g., $\mathcal{S}(^{0010}_{0010}\,|\,^{A}_{A})_{AA}$ and $\mathcal{S}(^{0001}_{0001}\,|\,^{A}_{A})_{AB}$. In calculations the contributions to an effective cross section are often expanded as a power series of the nonsphericitiy, β, of the interaction potential, like in the Distorted Wave Born Approximation (DWBA). Contributions to a cross section, where only the spherical part of the potential plays a role, i.e., zeroth order in β, can be calculated with the use of the well-known Chapman–Cowling-Ω integrals (see e.g., eqs. (19), (27) and (28)). In lowest order DWBA one can tell in most cases whether the contributions of a particular power in β are inelastic or not: e.g., in lowest order DWBA $\mathcal{S}(^{0200}_{0200}\,|\,^{A}_{A})_{AA}$ is quadratic in the nonsphericity, and has elastic contributions, whereas $\mathcal{S}(^{0200}_{2000}\,|\,^{A}_{A})_{AB}$ is quadratic in the nonsphericity and inelastic. Most cross sections that couple J-dependent polarizations to orientation independent polarizations are in lowest order DWBA linear in the nonsphericity, e.g., $\mathcal{S}(^{1001}_{1200}\,|\,^{A}_{A})_{AA}$, $\mathcal{S}(^{1010}_{1200}\,|\,^{A}_{A})_{AB}$, $\mathcal{S}(^{1000}_{1200}\,|\,^{A}_{A})_{AB}$; and some are quadratic in the nonsphericity and inelastic, e.g., $\mathcal{S}(^{1010}_{1200}\,|\,^{A}_{A})_{AA}$, $\mathcal{S}(^{0200}_{2000}\,|\,^{A}_{A})_{AB}$. The production cross sections for the odd in J polarizations are always of the latter type. In general the production cross sections are found to be small in comparison to diagonal cross sections. One has to bear in mind that the DWBA works well for molecules with small nonsphericity, e.g., H_2 and D_2, but can only give general trends for molecules like N_2: for instance $\mathcal{S}(^{0200}_{0200}\,|\,^{A}_{A})_{AA}$, although being quadratic in the nonsphericity, is comparable in magnitude to $\mathcal{S}(^{1010}_{1010}\,|\,^{A}_{A})_{AA}$, which has contributions from the spherical part of the potential. Usually, it is found that off-diagonal cross sections are small in comparison to diagonal ones.

Between various effective cross sections exact relations exist. These relations are listed in table VIII. For the mixtures they are mostly based on the work of Köhler and 't Hooft[24]). In our work $\Phi^{(1010)} = \sqrt{\frac{3}{5}}W(\frac{5}{2} - W^2)$ and $\Phi^{(0010)} = \sqrt{\frac{3}{2}}(\frac{3}{2} - W^2)$ are used, while in ref. 24 these polarizations have opposite sign. In table VIII those relations that differ for the two conventions are marked with [a]).

1) $\mathcal{S}(^{1000}_{1000}\,|\,^{A}_{A})_{AB}$.

This effective cross section is obtained from data on the field free diffusion coefficient (see section 9 and table VI). The contributions zeroth order in the nonsphericity (denoted with the symbol (0)) can be calculated with Ω integrals[25,26])

$$\mathcal{S}^{(0)}(^{1000}_{1000}\,|\,^{A}_{A})_{AB} = \mathcal{S}^{(0)}(^{1001}_{1001}\,|\,^{A}_{A})_{AB} = \mathcal{S}^{(0)}(^{1200}_{1200}\,|\,^{A}_{A})_{AB} = \mathcal{S}^{(0)}(^{1100}_{1100}\,|\,^{A}_{A})_{AB}$$
$$= \tfrac{4}{3}\pi \frac{m_B}{m_A + m_B} \sigma_{AB}^2 \Omega_{AB}^{(1,1)*}. \tag{27}$$

Using the potential parameters (σ, ϵ) of a 6–12 Lennard-Jones potential and

the combination rules $2\sigma_{AB} = \sigma_A + \sigma_B$ and $\epsilon_{AB} = \sqrt{\epsilon_A \epsilon_B}$, $\mathcal{S}^{(0)}$ can be calculated. The ratio of $\mathcal{S}^{(0)}(^{1000}_{1000}\,|\,^{A}_{A})_{AB}$ and $\mathcal{S}(^{1000}_{1000}\,|\,^{A}_{A})_{AB}$ is given in table VI and is close to unity for all systems under consideration. Thus the scattering processes in which only the spherical part of the potential plays a role – elastic processes – dominate the diffusion process. This has already been found by Mason and Monchick[43,38]).

2) $\mathcal{S}(^{1200}_{1200}\,|\,^{A}_{A})_{AA}$, $\mathcal{S}(^{1200}_{1200}\,|\,^{A}_{A})_{AB}$, $\mathcal{S}(^{1100}_{1100}\,|\,^{A}_{A})_{AA}$ and $\mathcal{S}(^{1100}_{1100}\,|\,^{A}_{A})_{AB}$.

These cross sections are obtained from the position on the B/p-axis of the $\overbrace{WJJ}$ and WJ polarizations (see section 7 and table V). In the case of mixtures the contributions proportional to β^0 are given in eq. (27). For the cross sections concerning AA collisions the zeroth order contributions in the nonsphericity are given by

$$\mathcal{S}^{(0)}(^{1200}_{1200}\,|\,^{A}_{A})_{AA} = \mathcal{S}^{(0)}(^{1100}_{1100}\,|\,^{A}_{A})_{AA} = \mathcal{S}^{(0)}(^{1001}_{1001}\,|\,^{A}_{A})_{AA} = \tfrac{2}{3}\pi\sigma_{AA}^2\Omega_{AA}^{(1,1)*}. \tag{28}$$

For $\mathcal{S}(^{1200}_{1200}\,|\,^{A}_{A})_{AA}$ an approximate relation[44]) exists in the high temperature limit for homonuclear diatomics with small nonsphericity:

$$\mathcal{S}(^{1200}_{1200}\,|\,^{A}_{A})_{AA} \simeq \mathcal{S}^{(0)}(^{1200}_{1200}\,|\,^{A}_{A})_{AA} + \tfrac{7}{6}\mathcal{S}(^{0200}_{0200}\,|\,^{A}_{A})_{AA}. \tag{29}$$

To check whether this relation holds and to investigate the possible existence of an analogous equation for the cross sections concerning AB collisions the following procedure is made: The difference between $\mathcal{S}(^{1200}_{1200}\,|\,^{A}_{A})_{kl}$ and $\mathcal{S}^{(0)}(^{1200}_{1200}\,|\,^{A}_{A})_{kl}$ is plotted against $\mathcal{S}(^{0200}_{0200})\,|\,^{A}_{A})_{kl}$, where $kl = AA$ or AB (fig. 29). The cross sections $\mathcal{S}^{(0)}(^{1200}_{1200}\,|\,^{A}_{A})_{kl}$ are calculated with Ω-integrals[26]) (see eqs. (27), (28) and table VI), while values for $\mathcal{S}(^{0200}_{0200}\,|\,^{A}_{A})_{kl}$ are taken from refs. 16 and 45 (see table V). As seen from the tables the spherical part of $\mathcal{S}(^{1200}_{1200}\,|\,^{A}_{A})_{kl}$ is dominant in the case of the hydrogen isotopes and accounts for about 50% or more in the case of N_2. This is explained by the fact that the nonsphericity of N_2 is much larger than for the hydrogen isotopes and the level splitting between different rotational states is less for N_2, making inelastic processes more probable. Fig. 29 shows that for most gases there is a correlation between $\{\mathcal{S}(^{1200}_{1200}\,|\,^{A}_{A})_{kl} - \mathcal{S}^{(0)}(^{1200}_{1200}\,|\,^{A}_{A})_{kl}\}$ and $\mathcal{S}(^{0200}_{0200}\,|\,^{A}_{A})_{kl}$, but that the factor arising in eq. (29) should be more close to unity than to 7/6. A similar result was found by Thijsse[7]). The cross sections which do not show such a correlation are those for pure HD and HD–Ar.

The values of $\mathcal{S}(^{1100}_{1100}\,|\,^{A}_{A})_{kl}$ are of the same order of magnitude as $\mathcal{S}(^{1200}_{1200}\,|\,^{A}_{A})_{kl}$, as expected since the contributions proportional to β^0 of $\mathcal{S}(^{1100}_{1100}\,|\,^{A}_{A})_{kl}$ are the same as for $\mathcal{S}(^{1200}_{1200}\,|\,^{A}_{A})_{kl}$ (eqs. (27) and (28)).

3) $\mathcal{S}(^{1000}_{1200}\,|\,^{A}_{A})_{AB}$ and $\mathcal{S}(^{1000}_{1100}\,|\,^{A}_{A})_{AB}$.

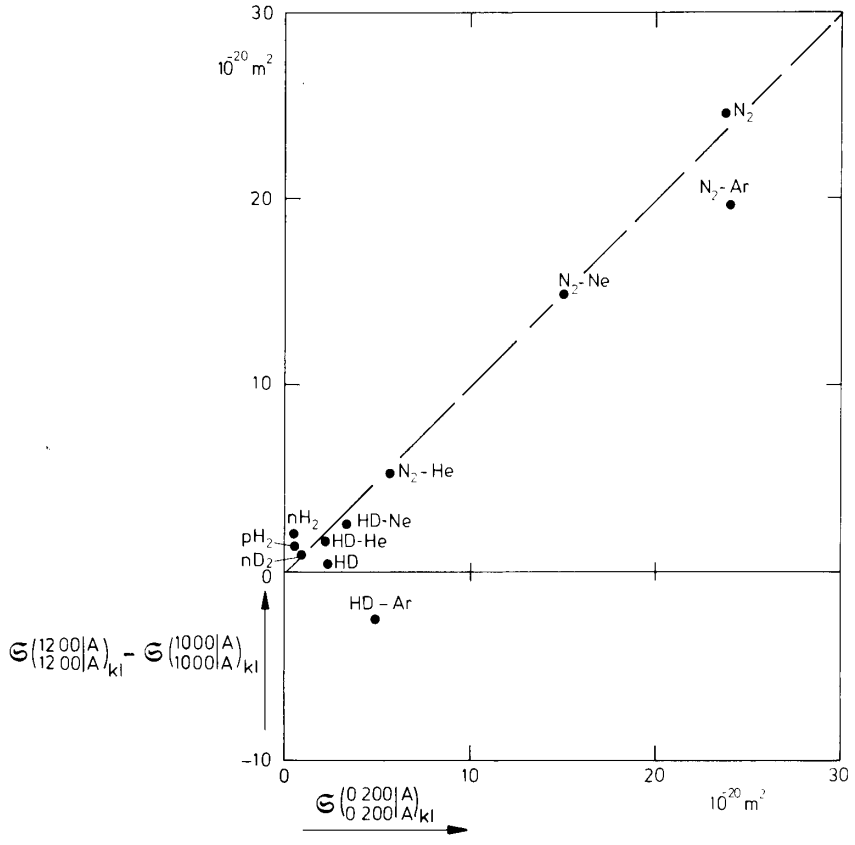

Fig. 29. $\{\mathcal{G}(^{1200}_{1200}|^{A}_{A})_{kl} - \mathcal{G}^{(0)}(^{1200}_{1200}|^{A}_{A})_{kl}\}$ versus $\mathcal{G}(^{0200}_{0200}|^{A}_{A})_{kl}$ for various systems. ($kl = AA$ or AB).

These cross sections govern the production of $\overline{WJJ}$ and WJ due to a particle flux. In lowest order DWBA $\mathcal{G}(^{1000}_{1100}|^{A}_{A})_{AB}$ is quadratic in the nonsphericity and only inelastic collisions contribute. For N_2 inelastic processes are more likely to happen than for the hydrogen isotopes. This explains why only in the case of N_2 mixtures a $\mathcal{G}(^{1000}_{1100}|^{A}_{A})_{AB}$ of a measurable size is found. In DWBA the main contributions to $\mathcal{G}(^{1000}_{1200}|^{A}_{A})_{AB}$ are linear in the nonsphericity. Hence it is understood that $\mathcal{G}(^{1000}_{1200}|^{A}_{A})_{AB}$ is larger than $\mathcal{G}(^{1000}_{1100}|^{A}_{A})_{AB}$ and the magnitude of these cross sections decreases going from N_2–noble gas, via HD–noble gas to H_2– and D_2–noble gas mixtures. According to eq. (259) of ref. 24, $\mathcal{G}(^{1000}_{1200}|^{A}_{A})_{AB}$ has a trivial $m_B/(m_A + m_B)$ mass dependence and will therefore increase going from He via Ne to Ar for one particular polyatomic gas. This is indeed found for N_2– and HD–noble gas systems, but not for H_2 and D_2–noble gas systems. In lowest order DWBA also $\mathcal{G}(^{1001}_{1200}|^{A}_{A})_{AA}$ known from $\lambda(B)$ measurements, is linear in the nonsphericity and has elastic

contributions. In view of this one expects $\mathcal{S}(^{1000}_{1200}\,|\,^{A}_{A})_{AB}$ to be of the same order of magnitude as $\mathcal{S}(^{1001}_{1200}\,|\,^{A}_{A})_{AA}$ (see eq. (A.2)). Experimentally one finds that the ratio between the two cross sections is 0.2 at the most (see table V). An explanation for this might be that collisions between a noble gas and a polyatomic gas (AB) do not align the polyatomic as easily as polyatomic–polyatomic (AA) collisions. An indication that $\mathcal{S}(^{1000}_{1200}\,|\,^{A}_{A})_{AB}$ is much smaller than $\mathcal{S}(^{1001}_{1200}\,|\,^{A}_{A})_{AA}$ is given by calculations of Sandler and Dahler[46]). Using a loaded sphere model they calculate the diffusion, the thermal diffusion and the thermal conductivity coefficients in the approximation that the $\overline{WJJ}$-polarization is to be neglected (the Pidduck approximation) and also by taking the $\overline{WJJ}$-polarization into account (as proposed by Kagan and Afanas'ev). From the difference between the two methods the Senftleben–Beenakker effect on the quantity studied can be estimated. In table VII the results of these calculations for an equimolar mixture of species with the same mass are displayed. It is seen that $\Delta\lambda/\lambda$ is about 5 times larger than $\Delta D_T/D$, which is 8 times larger than $\Delta D/D$. This implies an order of magnitude difference for $\mathcal{S}(^{1001}_{1200})$ and $\mathcal{S}(^{1000}_{1200}\,|\,^{A}_{A})_{AB}$.

Model calculations have been performed by Cooper, Dahler, Verlin, Matzen and Hoffman[47]) for thermal diffusion and diffusion in a magnetic field, which point to the same conclusion. They use a rigid ellipsoid model and for the equimolar N_2–Kr system with model parameters $\sigma_{Kr} = 1.805 \times 10^{-20}\,m^2$, $\sigma_{N_2} = 2.004 \times 10^{-20}\,m^2$ and $r_{N_2} = 1.154$, they obtain $(\Delta D_T^{\parallel}/D)_{sat} = 150 \times 10^{-6}$ and $(\Delta D^{\parallel}/D)_{sat} = 11 \times 10^{-6}$ (σ is the spherical size parameter and r is the ratio between the larger and smaller axis of the ellipsoid). The ratio between the

TABLE VII

Data for diffusion, thermal diffusion and thermal conductivity calculated with a loaded sphere model for an equimolar mixture of one species with excentricity e and a sphere according to ref. 46. The ratios of the masses is 1.

e [c])	nD [d])		D_T/x_Ax_Bd		λ [e])		$\frac{\Delta D}{D}\times 10^3$	$\frac{\Delta D_T}{D}\times 10^3$	$\frac{\Delta\lambda}{\lambda}\times 10^3$
	K.A. [a])	P [b])	K.A.	P	K.A.	P			
0.00	1.0172	1.0172	0.000	0.000	1.3200	1.3200			
0.05	1.0328	1.0328	0.0121	0.0112	1.3130	1.3116			
0.10	1.0484	1.0483	0.0295	0.0262	1.3143	1.3086	0.1	0.8	4

[a]) K.A.: Kagan-Afanas'ev approximation, in which contributions from $(\boldsymbol{W}\cdot\boldsymbol{J})\,\boldsymbol{J}$ are accounted for.

[b]) P: Pidduck approximation, in which contributions from $(\boldsymbol{W}\cdot\boldsymbol{J})\,\boldsymbol{J}$ are neglected.

[c]) $e = m\zeta^2/2\Gamma$ with m = mass, ζ is the displacement of the center of mass from the center of symmetry and Γ is the moment of inertia.

[d]) nD: is given in units of $(3/32\sigma^2)\,(kT/\pi m)^{1/2}$.

[e]) λ: is given in units of $(75/256\sigma^2)\,(k^3T/\pi m)^{1/2}$.

TABLE VIII
Exact relations between effective cross sections

Single component gases	Mixtures
$\mathfrak{S}\left(\begin{smallmatrix}0001\\pqrs\end{smallmatrix}\middle\vert\begin{smallmatrix}A\\A\end{smallmatrix}\right)_{AA} = \sqrt{\frac{3}{2}\frac{k}{C^A_{\rm rot}}}\,\mathfrak{S}\left(\begin{smallmatrix}0010\\pqrs\end{smallmatrix}\middle\vert\begin{smallmatrix}A\\A\end{smallmatrix}\right)_{AA}$ [a]	$-\sqrt{\tfrac{3}{2}}\mathfrak{S}\left(\begin{smallmatrix}0010\\pqrs\end{smallmatrix}\middle\vert\begin{smallmatrix}A\\A\end{smallmatrix}\right)_{AB} - \sqrt{\tfrac{3}{2}}\mathfrak{S}\left(\begin{smallmatrix}0010\\pqrs\end{smallmatrix}\middle\vert\begin{smallmatrix}B\\A\end{smallmatrix}\right)_{AB} + \sqrt{\frac{C^A_{\rm rot}}{k}}\,\mathfrak{S}\left(\begin{smallmatrix}0001\\pqrs\end{smallmatrix}\middle\vert\begin{smallmatrix}A\\A\end{smallmatrix}\right)_{AB} + \sqrt{\frac{C^B_{\rm rot}}{k}}\,\mathfrak{S}\left(\begin{smallmatrix}0001\\pqrs\end{smallmatrix}\middle\vert\begin{smallmatrix}B\\A\end{smallmatrix}\right)_{AB} = 0$ [a]
$\mathfrak{S}\left(\begin{smallmatrix}0001\\0001\end{smallmatrix}\middle\vert\begin{smallmatrix}A\\A\end{smallmatrix}\right)_{AA} = \frac{3}{2}\frac{k}{C^A_{\rm rot}}\,\mathfrak{S}\left(\begin{smallmatrix}0010\\0010\end{smallmatrix}\middle\vert\begin{smallmatrix}A\\A\end{smallmatrix}\right)_{AA} = +\sqrt{\frac{3k}{2C^A_{\rm rot}}}\,\mathfrak{S}\left(\begin{smallmatrix}0001\\0010\end{smallmatrix}\middle\vert\begin{smallmatrix}A\\A\end{smallmatrix}\right)_{AA}$ [a]	
$\mathfrak{S}\left(\begin{smallmatrix}1010\\1010\end{smallmatrix}\middle\vert\begin{smallmatrix}A\\A\end{smallmatrix}\right)_{AA} = \tfrac{2}{3}\mathfrak{S}\left(\begin{smallmatrix}2000\\2000\end{smallmatrix}\middle\vert\begin{smallmatrix}A\\A\end{smallmatrix}\right)_{AA} + \tfrac{5}{6}\mathfrak{S}\left(\begin{smallmatrix}0010\\0010\end{smallmatrix}\middle\vert\begin{smallmatrix}A\\A\end{smallmatrix}\right)_{AA}$	$\mathfrak{S}\left(\begin{smallmatrix}1010\\1010\end{smallmatrix}\middle\vert\begin{smallmatrix}A\\A\end{smallmatrix}\right)_{AB} + \left(\frac{m_B}{m_A}\right)^{3/2}\mathfrak{S}\left(\begin{smallmatrix}1010\\1010\end{smallmatrix}\middle\vert\begin{smallmatrix}A\\B\end{smallmatrix}\right)_{AB} = \tfrac{4}{3}\mathfrak{S}\left(\begin{smallmatrix}2000\\2000\end{smallmatrix}\middle\vert\begin{smallmatrix}A\\A\end{smallmatrix}\right)_{AB} + \tfrac{5}{3}\mathfrak{S}\left(\begin{smallmatrix}0010\\0010\end{smallmatrix}\middle\vert\begin{smallmatrix}A\\A\end{smallmatrix}\right)_{AB} - 3\mathfrak{S}\left(\begin{smallmatrix}1000\\1000\end{smallmatrix}\middle\vert\begin{smallmatrix}A\\A\end{smallmatrix}\right)_{AB}$
	$= \frac{4}{3}\frac{m_B}{m_A}\mathfrak{S}\left(\begin{smallmatrix}2000\\2000\end{smallmatrix}\middle\vert\begin{smallmatrix}A\\B\end{smallmatrix}\right)_{AB} + \frac{5}{3}\frac{m_B}{m_A}\mathfrak{S}\left(\begin{smallmatrix}0010\\0010\end{smallmatrix}\middle\vert\begin{smallmatrix}A\\B\end{smallmatrix}\right)_{AB} + 3\mathfrak{S}\left(\begin{smallmatrix}1000\\1000\end{smallmatrix}\middle\vert\begin{smallmatrix}A\\A\end{smallmatrix}\right)_{AB}$
	$\mathfrak{S}\left(\begin{smallmatrix}2000\\2000\end{smallmatrix}\middle\vert\begin{smallmatrix}A\\A\end{smallmatrix}\right)_{AB} - \frac{m_B}{m_A}\mathfrak{S}\left(\begin{smallmatrix}2000\\2000\end{smallmatrix}\middle\vert\begin{smallmatrix}A\\B\end{smallmatrix}\right)_{AB} = \mathfrak{S}\left(\begin{smallmatrix}0010\\0010\end{smallmatrix}\middle\vert\begin{smallmatrix}A\\A\end{smallmatrix}\right)_{AB} - \frac{m_B}{m_A}\mathfrak{S}\left(\begin{smallmatrix}0010\\0010\end{smallmatrix}\middle\vert\begin{smallmatrix}A\\B\end{smallmatrix}\right)_{AB} = 2\mathfrak{S}\left(\begin{smallmatrix}1000\\1000\end{smallmatrix}\middle\vert\begin{smallmatrix}A\\A\end{smallmatrix}\right)_{AB}$
$\mathfrak{S}\left(\begin{smallmatrix}1010\\1001\end{smallmatrix}\middle\vert\begin{smallmatrix}A\\A\end{smallmatrix}\right)_{AA} = +\tfrac{1}{2}\sqrt{\tfrac{5}{3}}\mathfrak{S}\left(\begin{smallmatrix}0010\\0001\end{smallmatrix}\middle\vert\begin{smallmatrix}A\\A\end{smallmatrix}\right)_{AA}$	$\mathfrak{S}\left(\begin{smallmatrix}1010\\1001\end{smallmatrix}\middle\vert\begin{smallmatrix}A\\A\end{smallmatrix}\right)_{AB} + \left(\frac{m_B}{m_A}\right)^{3/2}\mathfrak{S}\left(\begin{smallmatrix}1010\\1001\end{smallmatrix}\middle\vert\begin{smallmatrix}B\\A\end{smallmatrix}\right)_{AB} = +\sqrt{\tfrac{5}{3}}\mathfrak{S}\left(\begin{smallmatrix}0010\\0001\end{smallmatrix}\middle\vert\begin{smallmatrix}A\\A\end{smallmatrix}\right)_{AB}$
	$\mathfrak{S}\left(\begin{smallmatrix}0010\\0001\end{smallmatrix}\middle\vert\begin{smallmatrix}A\\A\end{smallmatrix}\right)_{AB} = \frac{m_B}{m_A}\mathfrak{S}\left(\begin{smallmatrix}0010\\0001\end{smallmatrix}\middle\vert\begin{smallmatrix}B\\A\end{smallmatrix}\right)_{AB}$
	$\mathfrak{S}\left(\begin{smallmatrix}1000\\pqrs\end{smallmatrix}\middle\vert\begin{smallmatrix}A\\A\end{smallmatrix}\right)_{AB} = -\sqrt{\frac{m_B}{m_A}}\,\mathfrak{S}\left(\begin{smallmatrix}1000\\pqrs\end{smallmatrix}\middle\vert\begin{smallmatrix}B\\A\end{smallmatrix}\right)_{AB}$, $\mathfrak{S}\left(\begin{smallmatrix}1000\\1010\end{smallmatrix}\middle\vert\begin{smallmatrix}A\\A\end{smallmatrix}\right)_{AB} = -\left(\frac{m_B}{m_A}\right)^{3/2}\mathfrak{S}\left(\begin{smallmatrix}1000\\1010\end{smallmatrix}\middle\vert\begin{smallmatrix}A\\B\end{smallmatrix}\right)_{AB}$
$\mathfrak{S}\left(\begin{smallmatrix}1010\\1200\end{smallmatrix}\middle\vert\begin{smallmatrix}A\\A\end{smallmatrix}\right)_{AA} = -\tfrac{1}{5}\sqrt{5}\,\mathfrak{S}\left(\begin{smallmatrix}0200\\2000\end{smallmatrix}\middle\vert\begin{smallmatrix}A\\A\end{smallmatrix}\right)_{AA}$ [a]	$\mathfrak{S}\left(\begin{smallmatrix}1010\\1200\end{smallmatrix}\middle\vert\begin{smallmatrix}A\\A\end{smallmatrix}\right)_{AB} + \left(\frac{m_B}{m_A}\right)^{3/2}\mathfrak{S}\left(\begin{smallmatrix}1010\\1200\end{smallmatrix}\middle\vert\begin{smallmatrix}B\\A\end{smallmatrix}\right)_{AB} = -\tfrac{2}{5}\sqrt{5}\,\mathfrak{S}\left(\begin{smallmatrix}0200\\2000\end{smallmatrix}\middle\vert\begin{smallmatrix}A\\A\end{smallmatrix}\right)_{AB}$ [a]
	$\mathfrak{S}\left(\begin{smallmatrix}0200\\2000\end{smallmatrix}\middle\vert\begin{smallmatrix}A\\B\end{smallmatrix}\right)_{AB} = \frac{m_A}{m_B}\mathfrak{S}\left(\begin{smallmatrix}0200\\2000\end{smallmatrix}\middle\vert\begin{smallmatrix}A\\A\end{smallmatrix}\right)_{AB}$
	$\mathfrak{S}\left(\begin{smallmatrix}2100\\2000\end{smallmatrix}\middle\vert\begin{smallmatrix}A\\A\end{smallmatrix}\right)_{AB} - \frac{m_B}{m_A}\mathfrak{S}\left(\begin{smallmatrix}2100\\2000\end{smallmatrix}\middle\vert\begin{smallmatrix}A\\B\end{smallmatrix}\right)_{AB} = 2\mathfrak{S}\left(\begin{smallmatrix}1100\\1000\end{smallmatrix}\middle\vert\begin{smallmatrix}A\\A\end{smallmatrix}\right)_{AB}$
$\mathfrak{S}\left(\begin{smallmatrix}1100\\1010\end{smallmatrix}\middle\vert\begin{smallmatrix}A\\A\end{smallmatrix}\right)_{AA} = 0$	$\mathfrak{S}\left(\begin{smallmatrix}1100\\1010\end{smallmatrix}\middle\vert\begin{smallmatrix}A\\B\end{smallmatrix}\right)_{AB} = -\left(\frac{m_A}{m_B}\right)^{3/2}\mathfrak{S}\left(\begin{smallmatrix}1100\\1010\end{smallmatrix}\middle\vert\begin{smallmatrix}A\\A\end{smallmatrix}\right)_{AB}$

[a] $\Phi^{(1010|k)} = \sqrt{\frac{4}{5}}\,W_k(\frac{5}{2} - W_k^2)$ and $\Phi^{(0010|k)} = \sqrt{\frac{2}{3}}(\frac{3}{2} - W^2)$.

two field effects is 15, pointing to a similar ratio for the two cross sections under consideration.

It should be remarked that in DWBA $\mathcal{S}(^{1010}_{1200}\,|\,^{A}_{A})_{AB}$ and $\mathcal{S}(^{1010}_{1200}\,|\,^{B}_{A})_{AB}$ are linearly proportional to the nonsphericity and have elastic contributions, in contrast to $\mathcal{S}(^{1010}_{1200}\,|\,^{A}_{A})_{AA}$. This means that it is not evident that B from eq. (17) should be much less than A from eq. (16) and omitting B in the analysis of the thermal conductivity change of mixtures as done in the literature[7,15]) is certainly not justified. A reanalysis of the data on Ψ^{λ}_{12} is given in the appendix.

11. Prediction of the field influence on diffusion

From eq. (21) it is seen that when both the thermal diffusion change and the thermal conductivity change are known and only one J-dependent polarization plays a role, the magnitude of the diffusion change can be calculated. Here, no approximations have to be made about off-diagonal cross sections. In fact, the formula remains valid for any number of orientation independent trial functions. For the systems for which the concentration dependence of both $\boldsymbol{D}_{\mathrm{T}}(B)$ and $\boldsymbol{\lambda}(B)$ are measured (N_2–noble gas and HD–noble gas systems) Ψ^{D}_{12} is calculated with the aid of eq. (21). For the mixtures of H_2 and D_2 with the noble gases Ar, Ne and He, however, no data on the concentration dependence of $\boldsymbol{\lambda}(B)$ is available. For these systems Ψ^{D}_{12} is calculated using eq. (15), where off-diagonal cross sections have been neglected with respect to diagonal ones. The cross sections needed for this calculation have been discussed in the former section. The resulting values for Ψ^{D}_{12} ($x_{\text{noble gas}} = \frac{1}{2}$) are given in table VI. These values are quite small. In a transverse type apparatus[13]), where D^{tr}/D is measured, one has

$$\delta x^{\mathrm{tr}} = \frac{l}{t}\frac{D^{\mathrm{tr}}}{D}\Delta x. \tag{30}$$

With the geometry factor $l/t \simeq 1$, $\Delta x = 0.2$ and $(D^{\mathrm{tr}}/D)_{\max}$ of 1×10^{-4} for an equimolar N_2–noble gas system, the transverse concentration difference would be 2×10^{-5}. (The smallest concentration difference detectable with the technique used here is about 2×10^{-6}.) As an example Ψ^{D}_{12} for N_2–He has been calculated over the entire concentration range and is plotted in fig. 30. The trivial concentration dependence (linearly proportional to $x_{\text{noble gas}}$) is clear. The deviation from the straight line is caused by the difference between $v_{AA}\mathcal{S}(^{1200}_{1200}\,|\,^{A}_{A})_{AA}$ and $v_{AB}\mathcal{S}(^{1200}_{1200}\,|\,^{A}_{A})_{AB}$.

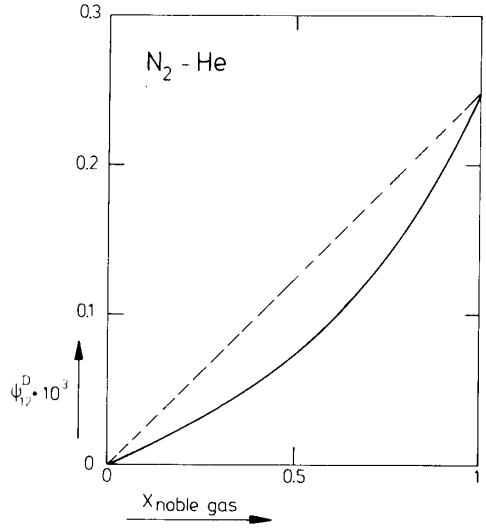

Fig. 30. Calculated concentration dependence of the diffusiomagnetic effect for N_2–He.

Appendix

In this section a new way of analyzing the results on the influence of a magnetic field on the thermal conductivity of a polyatomic noble gas mixture will be given. Here the coupling between $\boldsymbol{WJJ}$ and translational heat flux will not be neglected in contrast to former treatments[7,15]). It will be applied to the data of N_2–Ar, N_2–Ne, N_2–He, HD–Ar, HD–Ne and HD–He at room temperature as obtained by Heemskerk et al.[15]). Eq. (13) for Ψ_{12}^{λ} is rewritten as

$$
\begin{aligned}
F(x_B) \equiv & \sqrt{\frac{\lambda \Psi_{12}^{\lambda}}{x_A} \frac{2m_A}{k^2 T} \{x_A v_{AA} \mathfrak{S}(^{1200}_{1200} \mid ^{A}_{A})_{AA} + x_B v_{AB} \mathfrak{S}(^{1200}_{1200} \mid ^{A}_{A})_{AB}\}} \\
& \times \{x_A v_{AA} \mathfrak{S}(^{1001}_{1001} \mid ^{A}_{A})_{AA} + x_B v_{AB} \mathfrak{S}(^{1001}_{1001} \mid ^{A}_{A})_{AB}\} \\
= & \sqrt{\frac{C_{\mathrm{rot}}^{A}}{k}} \{x_A v_{AA} \mathfrak{S}(^{1001}_{1200} \mid ^{A}_{A})_{AA} + x_B v_{AB} \mathfrak{S}(^{1001}_{1200} \mid ^{A}_{A})_{AB}\} \\
& - \sqrt{\tfrac{5}{2}} B \{x_A v_{AA} \mathfrak{S}(^{1001}_{1001} \mid ^{A}_{A})_{AA} + x_B v_{AB} \mathfrak{S}(^{1001}_{1001} \mid ^{A}_{A})_{AB}\}. \qquad \text{(A.1)}
\end{aligned}
$$

B is given in eq. (17). There appear apart from decay cross sections only 5 different production cross sections: $\mathfrak{S}(^{1001}_{1200} \mid ^{A}_{A})_{kl}$, $\mathfrak{S}(^{1010}_{1200} \mid ^{A}_{A})_{kl}$ with $kl = AA$ or AB and $\mathfrak{S}(^{1010}_{1200} \mid ^{B}_{A})_{AB}$. The cross sections $\mathfrak{S}(^{1001}_{1200} \mid ^{A}_{A})_{AA}$ and $\mathfrak{S}(^{1010}_{1200} \mid ^{A}_{A})_{AA}$ are known for measurements on pure polyatomic gases[27]), (see also table V). For $\mathfrak{S}(^{1001}_{1200} \mid ^{A}_{A})_{AB}$ a fairly good estimate is obtained using the approximate relation derived by Köhler (eq. (266) of ref. 24)

$$\mathcal{S}\left(\begin{smallmatrix}1001\\1200\end{smallmatrix}\middle|\begin{smallmatrix}A\\A\end{smallmatrix}\right)_{AB} \approx \frac{1}{\langle \mathscr{E}_A \rangle_0}\sqrt{\frac{\overline{C_{\mathrm{rot}}^A}}{k}}\,\mathcal{S}\left(\begin{smallmatrix}1000\\1200\end{smallmatrix}\middle|\begin{smallmatrix}A\\A\end{smallmatrix}\right)_{AB}. \tag{A.2}$$

This relation strictly holds for those elastic contributions that are first order in the nonsphericity in DWBA. Thus $\mathcal{S}\left(\begin{smallmatrix}1001\\1200\end{smallmatrix}\middle|\begin{smallmatrix}A\\A\end{smallmatrix}\right)_{AB}$ is known from the thermal diffusion change in a field. Between the two remaining production cross sections an exact relation exists (see table VIII)

$$\mathcal{S}\left(\begin{smallmatrix}1010\\1200\end{smallmatrix}\middle|\begin{smallmatrix}B\\A\end{smallmatrix}\right)_{AB} = -\left(\frac{m_A}{m_B}\right)^{3/2}\left[\mathcal{S}\left(\begin{smallmatrix}1010\\1200\end{smallmatrix}\middle|\begin{smallmatrix}A\\A\end{smallmatrix}\right)_{AB} + \tfrac{2}{5}\sqrt{5}\,\mathcal{S}\left(\begin{smallmatrix}0200\\2000\end{smallmatrix}\middle|\begin{smallmatrix}A\\A\end{smallmatrix}\right)_{AB}\right]. \tag{A.3}$$

The cross section $\mathcal{S}\left(\begin{smallmatrix}0200\\2000\end{smallmatrix}\middle|\begin{smallmatrix}A\\A\end{smallmatrix}\right)_{AB}$ was determined by Burgmans et al.[16]) (see also table V) in the study of the viscomagnetic effect on mixtures. The two decay cross sections $\mathcal{S}\left(\begin{smallmatrix}1200\\1200\end{smallmatrix}\middle|\begin{smallmatrix}A\\A\end{smallmatrix}\right)_{kl}$ have been discussed in section 7. The seven cross sections $\mathcal{S}\left(\begin{smallmatrix}1010\\1010\end{smallmatrix}\middle|\begin{smallmatrix}i\\j\end{smallmatrix}\right)_{kl}$ and $\mathcal{S}\left(\begin{smallmatrix}1001\\1001\end{smallmatrix}\middle|\begin{smallmatrix}A\\A\end{smallmatrix}\right)_{kl}$ are calculated with Ω-integrals[25,26]) according to the following relations:

$$\begin{aligned}
\mathcal{S}^{(0)}\left(\begin{smallmatrix}1010\\1010\end{smallmatrix}\middle|\begin{smallmatrix}A\\A\end{smallmatrix}\right)_{AA} &= \tfrac{8}{15}\pi\sigma_A^2\Omega_{AA}^{(2,2)*},\\
\mathcal{S}^{(0)}\left(\begin{smallmatrix}1010\\1010\end{smallmatrix}\middle|\begin{smallmatrix}A\\A\end{smallmatrix}\right)_{AB} &= \frac{32}{15}\frac{m_B}{(m_A+m_B)^3}\{\tfrac{5}{16}(6m_A^2+5m_B^2)\Omega_{AB}^{(1,1)*}\\
&\qquad -\tfrac{15}{4}m_B^2\Omega_{AB}^{(1,2)*}+3m_B^2\Omega_{AB}^{(1,3)*}+m_Am_B\Omega_{AB}^{(2,2)*}\}\pi\sigma_{AB}^2,\\
\mathcal{S}^{(0)}\left(\begin{smallmatrix}1010\\1010\end{smallmatrix}\middle|\begin{smallmatrix}A\\B\end{smallmatrix}\right)_{AB} &= -\frac{32}{15}\frac{(m_Am_B)^{3/2}}{(m_A+m_B)^3}\{\tfrac{55}{16}\Omega_{AB}^{(1,1)*}-\tfrac{15}{4}\Omega_{AB}^{(1,2)*}+3\Omega_{AB}^{(1,3)*}-\Omega_{AB}^{(2,2)*}\}\pi\sigma_{AB}^2,
\end{aligned} \tag{A.4}$$

$$\begin{aligned}
\mathcal{S}^{(0)}\left(\begin{smallmatrix}1001\\1001\end{smallmatrix}\middle|\begin{smallmatrix}A\\A\end{smallmatrix}\right)_{AA} &= \tfrac{2}{3}\pi\sigma_A^2\Omega_{AA}^{(1,1)*},\\
\mathcal{S}^{(0)}\left(\begin{smallmatrix}1001\\1001\end{smallmatrix}\middle|\begin{smallmatrix}A\\A\end{smallmatrix}\right)_{AB} &= \tfrac{4}{3}\pi\frac{m_B}{m_A+m_B}\sigma_{AB}^2\Omega_{AB}^{(1,1)*}.
\end{aligned}$$

The experimental results for $F(x_B)$ as a function of noble gas mole fraction are fitted to the theory with only one adaptable parameter, $\mathcal{S}\left(\begin{smallmatrix}1010\\1200\end{smallmatrix}\middle|\begin{smallmatrix}A\\A\end{smallmatrix}\right)_{AB}$. The graphical results are displayed in fig. 31 for N_2–noble gas and in fig. 32 for the HD–noble gas systems. The values obtained for $\mathcal{S}\left(\begin{smallmatrix}1010\\1200\end{smallmatrix}\middle|\begin{smallmatrix}A\\A\end{smallmatrix}\right)_{AB}$ are listed in table V. It is clear from these data that the magnitude of Ψ_{12}^{λ} is for a significant part determined by the value of $B(x_B)$. Thus omitting the cross sections $\mathcal{S}\left(\begin{smallmatrix}1010\\1200\end{smallmatrix}\middle|\begin{smallmatrix}i\\j\end{smallmatrix}\right)_{kl}$ is certainly not justified. The reliability with which $\mathcal{S}\left(\begin{smallmatrix}1010\\1200\end{smallmatrix}\middle|\begin{smallmatrix}A\\A\end{smallmatrix}\right)_{AB}$ and $\mathcal{S}\left(\begin{smallmatrix}1010\\1200\end{smallmatrix}\middle|\begin{smallmatrix}B\\A\end{smallmatrix}\right)_{AB}$ are obtained depends strongly on the validity of eq. (A.2), which is a result of a DWBA calculation. The values of $\mathcal{S}\left(\begin{smallmatrix}1001\\1200\end{smallmatrix}\middle|\begin{smallmatrix}A\\A\end{smallmatrix}\right)_{AB}$ obtained from eq. (A.2) differ largely from those obtained in refs. 7 and 15.

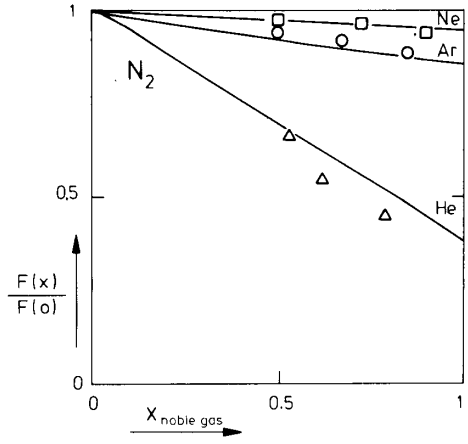

Fig. 31. The Senftleben–Beenakker effect on the thermal conductivity versus noble gas mole fraction for N_2-noble gas mixtures displayed according to eq. (A.1).

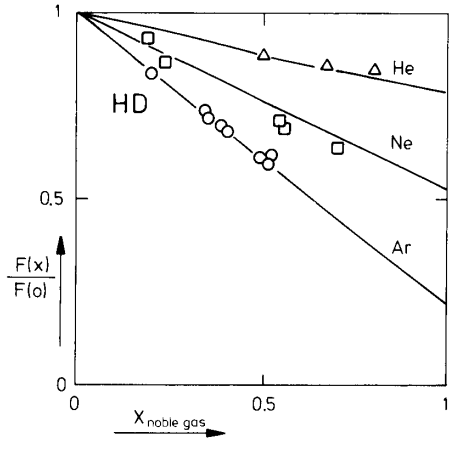

Fig. 32. The Senftleben–Beenakker effect on the thermal conductivity versus noble gas mole fraction for HD–noble gas mixtures displayed according to eq. (A.1).

Acknowledgements

Fruitful discussions with Dr. W.E. Köhler (University of Erlangen–Nürnberg) concerning the exact relations between the various effective molecular cross sections are gratefully acknowledged.

This work is part of the research program of the "Stichting voor Fundamenteel Onderzoek der Materie (FOM)" and has been made possible by financial support from the "Nederlandse Organisatie voor Zuiver-Wetenschappelijk Onderzoek (ZWO)".

References

1) J.J.M. Beenakker and F.R. McCourt, Annu. Rev. Phys. Chem. **21** (1970) 47.
2) J.J.M. Beenakker, H.F.P. Knaap and B.C. Sanctuary, AIP Conference Proc. **11** (1973) p. 21.
3) J.J.M. Beenakker, Lecture Notes in Physics **31** (Springer-Verlag, Berlin, 1974) p. 413.
4) J.A.R. Coope and R.F. Snider, J. Chem. Phys. **56** (1972) 2056; ibid **57** (1972) 4266.
5) H. Moraal, Phys. Rep. **17C** (1975) 225.
6) P.G. van Ditzhuyzen, B.J. Thijsse, L.K. van der Meij, L.J.F. Hermans and H.F.P. Knaap, Physica **88A** (1977) 53.
7) B.J. Thijsse, Thesis, University of Leiden, 1978; Physica, to be published.
8) A. Tip, A.E. de Vries and J. Los, Physica **32** (1966) 1429.
9) M.A. Hidalgo, J.M. Saviron and D. Gonzalez, Physica **46** (1970) 41.
10) H. Senftleben and H. Schult, Ann. Physik **7** (1950) 103.
11) H.F. Vugts, A. Tip and J. Los, Physica **38** (1968) 579.
12) V.D. Borman, B.I. Nikolaev, N.I. Nikolaev, V.A. Chuzhinov, Zh. Eksp. Teor. Fiz. **60** (1971) 1627, Sov. Phys. JETP **33** (1971) 881.
13) E. Mazur, to be published.
14) K.E. Grew and T.L. Ibbs, Thermal Diffusion in Gases (Cambridge Univ. Press, London, 1952).
15) J.P.J. Heemskerk, G.F. Bulsing and H.F.P. Knaap, Physica **71** (1974) 515.
16) A.L.J. Burgmans, P.G. van Ditzhuyzen and H.F.P. Knaap, Z. Naturforsch. **28a** (1973) 849.
17) G.E.J. Eggermont, H. Vestner and H.F.P. Knaap, Physica **82A** (1976) 23.
18) Yu. Kagan and L.A. Maksimov, Sov. Phys. JETP **24** (1967) 1272.
19) W.E. Köhler and J. Halbritter, Z. Naturforsch. **30a** (1975) 1114.
20) V.D. Borman, B.I. Nikolaev and N.I. Nikolaev, Sov. Phys. JETP **24** (1967) 387.
21) J. Monchick, S.I. Sandler and E.A. Mason, J. Chem. Phys. **49** (1968) 1178.
22) L.J.F. Hermans, J.M. Koks, A.F. Hengeveld and H.F.P. Knaap, Physica **50** (1970) 410.
23) J.J. de Groot, J.W. van den Broeke, H.J. Martinius, C.J.N. van den Meijdenberg and J.J.M. Beenakker, Physica **56** (1971) 388.
24) W.E. Köhler and G.W. 't Hooft, Z. Naturforsch., in press.
25) S. Chapman and T.G. Cowling, The Mathematical Theory of Nonuniform Gases (Cambridge Univ. Press, London, 1970).
26) J.O. Hirschfelder, C.F. Curtiss and R.B. Bird, The Molecular Theory of Gases and Liquids (John Wiley, New York, 1954).
27) J.P.J. Heemskerk, F.G. van Kuik, H.F.P. Knaap and J.J.M. Beenakker, Physica **71** (1974) 484.
28) W.E. Köhler and H.F.P. Knaap, Z. Naturforsch. **31a** (1976) 1485.
29) A. Tip, Physica **37** (1967) 82.
30) H. Hulsman, G.F. Bulsing, G.E.J. Eggermont, L.J.F. Hermans and J.J.M. Beenakker, Physica **72** (1974) 287.
31) G.E.J. Eggermont, P. Oudemann, L.J.F. Hermans and J.J.M. Beenakker, Physica **91A** (1978) 345.
32) H. van Ee, Thesis, University of Leiden, 1966.
33) Yu. Kagan and L.A. Maksimov, Sov. Phys. JETP **14** (1962) 604.
34) J. Malone, Thesis, Harvard University, Cambridge, 1972.
35) H. Cauwenbergh and W. van Dael, Physica **54** (1971) 347.
36) A.K. Barua, Indian J. Phys. **34** (1960) 169.
37) J.M. Gandhi and S.C. Saxena, Br. J. Appl. Phys. **18** (1967) 807.
38) E.A. Mason and T.R. Marrero, Adv. At. Mol. Phys. **6** (1970) 155.
39) B.A. Ivakin and P.E. Suetin, Zh. Tekh. Fiz. **33** (1963) 1007; Sov. Phys. Tech. Phys. **8** (1964) 748.
40) S. Weissman and E.A. Mason, J. Chem. Phys. **37** (1962) 1289.
41) A.S.M. Wahby, A.J.H. Boerboom and J. Los, Physica **74** (1974) 85.

42) K.R. Harris and T.N. Bell, Can. J. Phys. **51** (1973) 2101.
43) E.A. Mason and L. Monchick, J. Chem. Phys. **36** (1962) 2746.
44) H. Moraal and R.F. Snider, Chem. Phys. Lett. **9** (1971) 401.
45) P.G. van Ditzhuyzen, L.J.F. Hermans and H.F.P. Knaap, Physica **88A** (1977) 452.
46) S.I. Sandler and J.S. Dahler, J. Chem. Phys. **47** (1967) 2621.
47) E.R. Cooper, J.S. Dahler, J.D. Verlin, M.K. Matzen and D.K. Hoffman, J. Chem. Phys. **59** (1973) 403.
48) W.E. Köhler and G.E.J. Eggermont, Physica **91A** (1978) 17.

6.1. *Consistency tests*

It was verified that the measured transverse concentration difference is linear in ΔT and that no effects were observed performing experiments with noble gases. Secondly the orientation of the apparatus with respect to the magnetic field was checked by measuring the concentration difference as a function of the field orientation. In fig. 7 δx is plotted versus the angle χ (see fig. 4) for an equimolar N_2–Ar mixture with $B/p = 5.70$ mT/Pa and $(\Delta T/T) = 0.0341$. Fig. 7 can easily be understood if one bears in mind that the transport tensor $\boldsymbol{D}_T$ can also be expressed by

$$D_{T_{ik}} = D_T^{\perp}\delta_{ik} + (D_T^{/\!/} - D_T^{\perp})h_i h_k - D_T^{tr}\epsilon_{ikl}h_l,$$

where $\boldsymbol{h}$ is a unit vector in the direction of the magnetic field. When as in fig. 4, ∇T is in the z-direction and the magnetic field is varied according to $\boldsymbol{h} = (\sin\chi,\ \tfrac{1}{2}\sqrt{2}\cos\chi,\ -\tfrac{1}{2}\sqrt{2}\cos\chi)$, the concentration difference in the y-direction is given by $D_{T_{yz}}$, which is given by

$$\delta x = \frac{l}{t}\left[\sin\chi\,\frac{D_T^{tr}}{D} + \cos^2\chi\,\frac{D_T^{/\!/} - D_T^{\perp}}{2D}\right]\Delta \ln T. \tag{23}$$

At $\chi = \pi/2$ and $3\pi/2$ the quantity D_T^{tr}/D is determined, while at $\chi = 0$ and π the quantity $(D_T^{/\!/} - D_T^{\perp})/2D$ is found. As can be readily seen from fig. 7 a

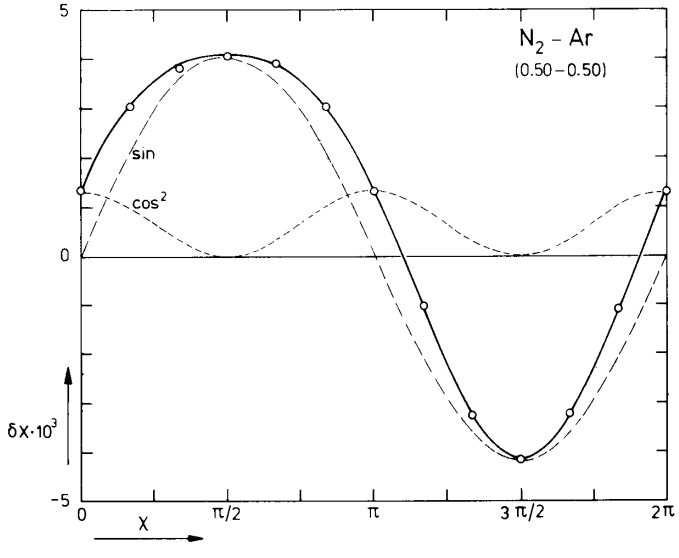

Fig. 7. The angle dependence of the observed transverse concentration gradient for N_2–Ar ($x_{\text{noble gas}} = 0.50$) at $B/p = 5.70$ mT/Pa and $\Delta T/T = 0.0341$. The dashed curves show the separate contribution from $D_T^{tr}(\sin\chi)$ and $(D_T^{/\!/} - D_T^{\perp})/2D(\cos^2\chi)$.

misalignment of the apparatus would seriously affect the value of $(D_T^{\parallel} - D_T^{\perp})/2D$ derived from the experimental values of δx and $\Delta T/T$, whereas D_T^{tr}/D would hardly be affected. Proper alignment is ensured by orienting the apparatus in such a way that the transverse concentration gradient observed at $\chi = 0$ and $\chi = \pi$ are the same within the limits of the experimental accuracy. It should be noted that the shape of a plot like fig. 7 depends very much on the parameter B/p. At low B/p values a function essentially proportional to $\sin\chi$ is obtained, whereas at large B/p values a function proportional to $\cos^2\chi$ is obtained (see fig. 2).

6.2. *Analysis of the experimental curves*

The experimental results of each system – corrected for Knudsen effects – are shown in figs. 8, 10 through 21, where double logarithmic plots of D_T^{tr}/D and $(D_T^{\parallel} - D_T^{\perp})/2D$ versus B/p are made. Results are shown for a particular concentration, the results at the other composition being quite analogous. The graphs show a unique B/p behavior.

The simplest approach to the experimental data is to fit them with the theoretical curves of eqs. (11) with $\Psi_{11}^T = 0$. For some systems, viz., N_2–Ar, N_2–Ne and D_2–He, large deviations are found for this one polarization ($\widehat{WJJ}$) theory. This is illustrated by the dotted line of fig. 8. There the dotted curve for D_T^{tr} is fitted to the experimental points (with Ψ_{12}^T and $B/p\xi_{12}$ as parameters) making the agreement for $(D_T^{\parallel} - D_T^{\perp})/2D$ rather poor. A second way to describe the experiments using one polarization is to abandon the spherical approximation, so that the experiments have to be fitted to the theoretical curves of eqs. (22). The dashed line in fig. 8 shows such a four parameter ($B/p\bar{\xi}_{12}$, a_2, a_3 and Ψ_{12}^T) fit made for the equimolar N_2–Ar mixture. The agreement between theory and experiment is quite good and the values found for the four parameters are: $B/p\bar{\xi}_{12} = 4.57$ mT/Pa, $a_2 = 0.727$, $a_3 = 1.36$ and $\Psi_{12}^T = 0.419 \times 10^{-3}$. However, complications arise when a comparison is made with the theoretical results of the thermal conductivity. As stated in section 3 the parameters $B/p\bar{\xi}_{12}$, a_2 and a_3, determining the shape of the transport coefficients over the entire B/p range, should be the same for $\boldsymbol{D}_T$ and $\boldsymbol{\lambda}$. Consequently, also the values of $(\Delta\lambda^{\perp}/\Delta\lambda^{\parallel})_{sat}$ and $(\Delta D_T^{\perp}/\Delta D_T^{\parallel})_{sat}$ should be the same. The value of $(\Delta\lambda^{\perp}/\Delta\lambda^{\parallel})_{sat}$ as determined by Heemskerk et al.[15]) from $\lambda^{\perp}$ and $\lambda^{\parallel}$ measurements in the presence of a magnetic field is about 1.64 for the equimolar N_2–Ar mixture. The corresponding value for $(\Delta D_T^{\perp}/\Delta D_T^{\parallel})_{sat}$ as calculated from the field parameters is equal to 1.35. This leads to the conclusion that the thermal conductivity and thermal diffusion measurements cannot be brought simultaneously into agreement with a single $\widehat{WJJ}$-polarization theory by dropping the spherical approximation. It is noted, that

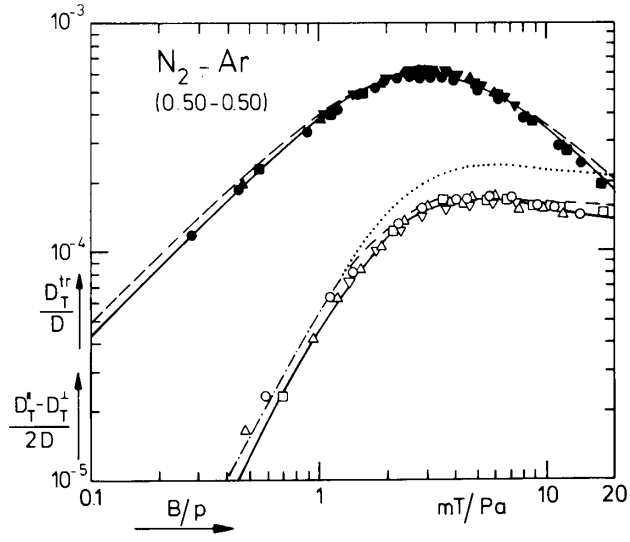

Fig.8. $D_T^{\parallel}/D$ and $(D_T^{\parallel} - D_T^{\perp})/2D$ versus B/p for N_2–Ar ($x_{\text{noble gas}} = 0.50$). ■□ 107 Pa; ●○ 133 Pa; ▲△ 161 Pa; ▼▽ 267 Pa; .... theoretical curves of $\overline{WJJ}$-polarization with the use of the spherical approximation (eqs. (11) with $\Psi_{11}^{T} = 0$). (The curve of D_T^{tr} fitted to the experimental points and happens to coincide with ——.); --- theoretical curves of eqs. (22) fitted to the experimental points ($\overline{WJJ}$-polarization without the spherical approximation); ——, theoretical curves of eqs. (11) fitted to the experimental points (both $\overline{WJJ}$ and WJ-polarizations are present and the spherical approximation is used).

when only the measurements of $\boldsymbol{D}_T(\boldsymbol{B})$ are considered an analysis with the use of eqs. (22) is consistent. This is seen in fig. 9, where the four parameters (Ψ_{12}^{T}, $\bar{\xi}_{12}$, $a_2\bar{\xi}_{12}$ and $a_3\bar{\xi}_{12}$) are plotted versus noble gas mole fraction for N_2–Ne and N_2–Ar. As expected from eqs. (22), the parameters $B/pa_l\bar{\xi}_{12}$ give straight lines which intersect at $x_{\text{noble gas}} = 0$. A third way of interpreting the thermal diffusion measurements is to introduce an extra polarization, viz., WJ. The theoretical curves for this case are given in eq. (11). A justification for the choice of WJ as the extra polarization is the fact that $(\Delta\lambda^{\perp}/\Delta\lambda^{\parallel})_{\text{sat}}$ for the N_2 – noble gas mixtures is slightly larger than 1.5[15]), which suggests the existence of a polarization odd in J. The next odd-in-J polarization available is $\overline{WWW}\,\overline{JJJ}$, which is less probably by its high tensorial rank. Indeed, by using a superposition of a dominant $\overline{WJJ}$ and a smaller WJ contribution agreement between the two experiments is now found as will be shown in the following sections. This procedure is also found to give a good fit to the present data (see figs. 8, 10 through 21). The fitting of the experimental points to the theoretical formulas is done by using a least squares method of Marquardt as supplied by the Nottingham Algorithms Group. The parameters Ψ_{12}^{T}, $B/p\xi_{12}$, Ψ_{11}^{T} and $B/p\xi_{11}$ obtained in this way are listed in table IV and will

mixture at pressures ranging from 100 to 270 Pa. The experimental data are almost a unique function of B/p, as expected (see eqs. (11), (12) and (22)). From fig. 5 it is clear that the magnitude of the effects depends slightly on the pressure. This is due to the finite dimensions of the apparatus. The Knudsen corrections on the magnitude of the effects were made according to

$$\frac{D_T^{tr}}{D} = \left(\frac{D_T^{tr}}{D}\right)_{meas} (1 + K/p),$$

$$\frac{D_T^{\parallel} - D_T^{\perp}}{2D} = \left(\frac{D_T^{\parallel} - D_T^{\perp}}{2D}\right)_{meas} (1 + K/p).$$

K is determined from the slope of e.g., $(D/D_T^{tr})_{meas}^{max}$ versus $1/p$. In fig. 6 such a plot is made for an equimolar N_2–Ar mixture. No Knudsen effects were found on the position on the B/p-axis. In table II the Knudsen constants for all the systems studied are given. The Knudsen constant on the magnitude of the thermal conductivity effect is a linear function of the noble gas concentration according to Heemskerk et al.[15]). Burgmans et al. claim that the inverse of the Knudsen constant for the viscomagnetic effect is linear in the concentration[16]). For the thermal diffusion effect, however, a simple concentration dependence of the Knudsen constant is not apparent. A possible explanation for this difference in behavior is that, in the case of thermal diffusion, there is

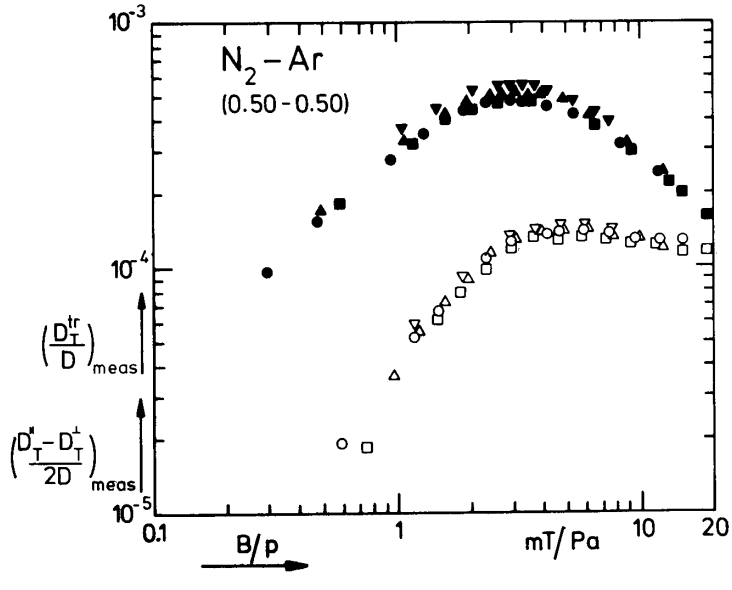

Fig. 5. D_T^{tr}/D (closed symbols) and $(D_T^{\parallel} - D_T^{\perp})/2D$ (open symbols) versus B/p for N_2–Ar ($x_{noble\ gas}$ = 0.50) at 300 K (no Knudsen corrections are applied). ■□ 107 Pa; ●○ 133 Pa; ▲△ 161 Pa; ▼▽ 267 Pa.

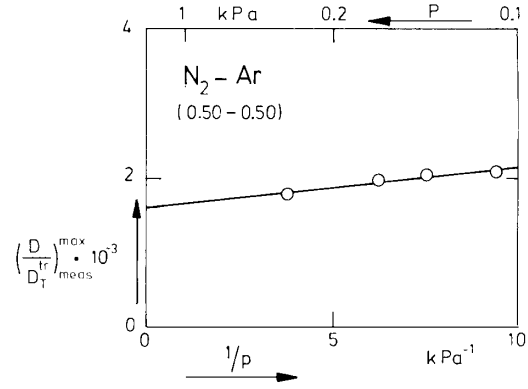

Fig. 6. Determination of the Knudsen coefficient K from the maximum of the transverse effect.

TABLE II

Mean free path correction constant K in Pa. These experimental constants contain both "pure" Knudsen effects and corrections for the thermomagnetic pressure difference (see text). In those cases where the Knudsen constants for D_T^{tr} and $D_T^{\parallel} - D_T^{\perp}$ were found to be significantly different, the latter values are given between parentheses.

	$x_{\text{noble gas}}$	N_2	HD	nH_2	nD_2	pH_2
He	0.25	< 5	125	40	81	
	0.50	24	35	55	59	
	0.75	11	88	56	53 (−30)	
	0.865				102 (−30)	
Ne	0.25	< 5	65	43	40	
	0.50	16	37	7	60	
	0.75	< 5	25	20	28	
Ar	0.125		< 5			
	0.25	< 5	13	55	31	73
	0.50	24	< 10	56	< 5	52
	0.75	< 5	< 5	41	45	36
	0.875	< 5				

a contribution from the thermomagnetic pressure difference: a transverse pressure difference across the channel proportional to $1/p$[30,31]). Due to the mean free path effects on the thermal conductivity this thermomagnetic pressure difference affects our measurements. It's contribution is largely suppressed by the geometry of our channel: $p\delta p/\Delta T \propto l/t^3$, which is in our case smaller by a factor 69 than in the case of refs. 30 and 31. Consequently, it's contribution, which depends on pressure as well as system, is only of the

order of a few percent of the total bridge unbalance. It is estimated by observing the unbalance for a pure polyatomic gas in a magnetic field, in which case no thermal diffusion is present. It should be stressed that corrections due to the thermomagnetic pressure difference are indistinguishable from "pure" Knudsen effects, since both have a $1/p$ behavior. Therefore, the numbers in table II have no other value than for extrapolating the experimental data to zero mean free path values.

Surprising experimental results for K are obtained for the system nD_2–He. When the mole fraction of the noble gas is 0.25 or 0.50 the magnitude of both the transverse thermal diffusion ratio as well as the difference between the two longitudinal components slightly increases with increasing pressure. However, when the He-mole fraction is 0.75 or 0.865 $-D_T^{tr}/D$ increases and $(D_T^{\parallel} - D_T^{\perp})/2D$ decreases with increasing pressure. The experimental results for the two effects are corrected to a high pressure limit with different Knudsen constants. In these cases the Knudsen constant for $(D_T^{\parallel} - D_T^{\perp})/2D$ is given in table II between parentheses. The reason for this strange behavior is not clear. A possible explanation might be that for these systems the thermomagnetic pressure difference is quite different for the two orientations of the magnetic field. The validity of this statement cannot be verified since the relative sign and magnitude of the thermomagnetic pressure difference for a polyatomic-noble gas mixture in the two field orientations is not yet known.

6. Experimental results

Experiments were performed at 300 K on the systems N_2–Ar, N_2–Ne, N_2–He, pH_2–Ar, nH_2–Ar, nH_2–Ne, nH_2–He, nD_2–Ar, nD_2–Ne, nD_2–He, HD–Ar, HD–Ne and HD–He. All gases, except HD, were obtained commercially and their purities are listed in table III. HD was prepared using the reaction

$$LiAlH_4 + 4D_2O \rightarrow LiOD + Al(OD)_3 + 4HD.$$

The small quantities H_2 and D_2 that are present in the product gas were removed using a rectification column as described by van Ee[32]). D_2 was also fractionally distilled at 20 K to remove isotopic impurities (like HD).

TABLE III

Purity of the gases			
N_2	99.99%	He	99.995%
H_2	99.9%	Ne	99.99%
HD	99% (isotropic)	Ar	99.99%
D_2	99.6% (isotropic)		